Development/Plasticity/Repair

Differential Postnatal Maturation of $GABA_A$, Glycine Receptor, and Mixed Synaptic Currents in Renshaw Cells and Ventral Spinal Interneurons

David González-Forero and Francisco J. Alvarez
Department of Anatomy and Physiology, Wright State University, Dayton, Ohio 45435

Renshaw cells (RCs) receive excitatory inputs from motoneurons to which then they inhibit. The gain of this spinal recurrent inhibitory circuit is modulated by inhibitory synapses on RCs. Inhibitory synapses on RCs mature postnatally, developing unusually large postsynaptic gephyrin clusters that colocalize glycine and $GABA_A$ receptors. We hypothesized that these features potentiate inhibitory currents in RCs. Thus, we analyzed glycinergic and GABAergic "inhibitory" miniature postsynaptic currents (mPSCs) in neonatal [postnatal day 1 (P1) to P5] and mature (P9–P15) RCs and compared them to other ventral interneurons (non-RCs). Recorded neurons were Neurobiotin filled and identified as RCs or non-RCs using *post hoc* immunohistochemical criteria. Glycinergic, GABAergic, and mixed glycine/GABA mPSCs matured differently in RCs and non-RCs. In RCs, glycinergic and $GABA_A$ mPSC peak amplitudes increased 230 and 45%, respectively, from P1–P5 to P9–P15, whereas in non-RCs, glycinergic peak amplitudes changed little and $GABA_A$ amplitudes decreased. $GABA_A$ mPSCs were slower in RCs (P1–P5, $\tau = 58$ ms; P9–P15, $\tau = 43$ ms) compared with non-RCs (P1–P5, $\tau = 27$ ms; P9–P15, $\tau = 14$ ms). Thus, fast glycinergic currents dominated "mixed" mPSC peak amplitudes in mature RCs, and $GABA_A$ currents dominated their long decays. In non-RCs, GABAergic and mixed events had shorter durations, and their frequencies decreased with development. Functional maturation of inhibitory synapses on RCs correlates well with increased glycine receptor recruitment to large gephyrin patches, colocalization with $\alpha 3/\alpha 5$-containing $GABA_A$ receptors, and maintenance of GABA/glycine corelease. As a result, charge transfer in GABA, glycine, or mixed mPSCs was larger in mature RCs than in non-RCs, suggesting RCs receive potent inhibitory synapses.

Key words: **development; subunit composition; corelease; gephyrin; GABA; synapse; motor**

Introduction

Inhibitory synapses develop a large variety of functional, structural, and molecular properties to counteract synaptic excitation and shape-firing patterns. These characteristics adjust inhibitory current amplitudes and timing to the integration properties of neurons and synaptic networks (Browne et al., 2001; Pouille and Scanziani, 2001; Semyanov et al., 2004). They also homeostatically regulate the balance between synaptic excitation and inhibition (Turrigiano and Nelson, 2004). The number and position of inhibitory synapses along dendritic arbors, the amount of GABA or glycine released or coreleased, and the characteristics of postsynaptic neurotransmitter actions influence postsynaptic currents, and all are developmentally regulated. Postsynaptic actions are in turn dependent on the number and properties of $GABA_A$ and glycine receptors. Postsynaptic receptor selection results in synapses that are mainly glycinergic, others GABAergic, and some mixed (Jonas et al., 1998; Kotak et al., 1998; O'Brien and Berger, 1999; Smith et al., 2000; Gao et al., 2001; Keller et al., 2001; Nabekura et al., 2004). These neurotransmitter/receptor choices greatly influence inhibition strength and timing (Russier et al., 2002). GABAergic transmission predominates over glycinergic transmission during early development, when both neurotransmitters depolarize neurons. Thereafter, the balance switches to glycine-dominated transmission in many spinal and brainstem synapses. The present consensus is that GABAergic currents are more efficient triggering long depolarizations and calcium entry related to developmental mechanisms, including synaptic formation and stabilization. Thereafter, inhibitory synapses shift their function to synaptic integration, and a bias toward "faster" glycinergic mechanisms seems advantageous for many ventral spinal cord synapses. $GABA_A$ receptor recruitment influences GABAergic current amplitudes (Nusser et al., 1997, 1998), and their time course is strongly related to subunit composition (Browne et al., 2001; Vicini et al., 2001). Glycinergic currents show an interesting property in that postsynaptic current amplitude is correlated with the amount of postsynaptic gephyrin (Lim et al., 1999; Van Zundert et al., 2004), a glycine receptor-anchoring protein (Kirsch and Betz, 1993; Feng et al., 1998; Meier et al., 2000, 2001).

One type of spinal interneuron, the Renshaw cell (RC), stands out because it displays a high density of proximal inhibitory synapses with large postsynaptic densities intensely immunoreactive

Received June 16, 2004; revised Jan. 4, 2005; accepted Jan. 6, 2005.

This work was supported by National Science Foundation Grant 9984441 to F.J.A. D.G.-F. was supported by a postdoctoral fellowship from the Ministerio de Educación, Cultura y Deporte (Spain). We thank Drs. Javier Stern and Bruce Walsmley for technical advice and helpful comments and suggestions on a previous version of this manuscript.

Correspondence should be addressed to Dr. Francisco J. Alvarez, Department of Anatomy and Physiology, Wright State University, 3640 Colonel Glenn Highway, Dayton, OH 45435. E-mail:francisco.alvarez@wright.edu.

DOI:10.1523/JNEUROSCI.2383-04.2005

 0270-6474/05/252010-14$15.00/0

to gephyrin and containing colocalized $GABA_A$ and glycine receptors (Alvarez et al., 1997; Geiman et al., 2002). These receptors are postsynaptic to boutons expressing markers, suggesting significant GABA/glycine corelease. We hypothesized that these structural and neurochemical properties increase synaptic inhibition by simultaneously enhancing peak amplitudes and time courses of postsynaptic currents (Geiman et al., 2002). These characteristics are likely adapted to RC function because, unlike other interneurons, they receive motor axon excitatory inputs of large amplitude and long duration that evoke high-frequency burst firing (Renshaw, 1946; Eccles et al., 1954). Synaptic structure on RCs matures postnatally in conjunction with ventral horn motor output and locomotion (Geiman et al., 2000). To investigate functional features characteristic of inhibitory synapses on RCs, we analyzed the amplitude and time courses of spontaneous miniature inhibitory currents and their GABAergic and glycinergic components during postnatal development and compared them to other ventral interneurons of similar ages.

Materials and Methods

Tissue preparation and immunohistochemical processing. The distribution, density, and immunocytochemical properties of RCs were analyzed in spinal cord sections obtained from early [postnatal day 1 (P1), P5] and late (P10, P15) postnatal rat spinal cords. This information was then used to target our recordings to a specific area of the spinal cord containing high densities of RCs and to classify recorded cells as "Renshaw" (RC) or "non-Renshaw" (non-RC) using *post hoc* immunohistochemistry.

For histological processing, a total of 12 pups (three rats in each age group) were used. Rats were anesthetized with an overdose of sodium pentobarbital (>90 mg/kg, i.p.) and perfused transcardially with cold vascular rinse (0.01 M phosphate buffer with 137 mM NaCl, 3.4 mM KCl, and 6 mM $NaHCO_3$, pH 7.3), followed by fixative (4% paraformaldehyde in 0.1 M phosphate buffer). Spinal cords were removed, postfixed for 1 h at room temperature, and cryoprotected at 4°C in 0.1 M phosphate buffer with 15% sucrose. Twenty-micrometer-thick transverse sections were obtained on a cryostat from L4–L5 spinal cord segments and collected on slides. Some sections were dual immunolabeled for neuronal nuclear protein (NeuN) [mouse monoclonal antibody (mAb); Chemicon, Temecula, CA], a generalized neuronal marker, and for calbindin [rabbit polyclonal antibody (pAb); Swant, Bellinzona, Switzerland], an RC marker in the ventral horn of the developing spinal cord (Geiman et al., 2000). In other sections, these markers were combined with immunostaining for the vesicular acetylcholine transporter (VAChT) (goat pAb; PharMingen, San Diego, CA). Different dual or triple immunolabelings were used to map the distribution of RCs to estimate their density in ventral horn regions targeted for recording (see Fig. 1*A*, *B*) and to analyze the competence of criteria for distinguishing RCs from neighboring non-RC interneurons in neonatal rat spinal cord based on the presence of abundant "cholinergic contacts" (see Fig. 1*C–F*).

The sections were washed in 0.01 M phosphate buffer containing 0.9% saline and 0.1% Triton X-100 (PBS/TX) and blocked with normal horse serum (NHS) (1:10 in PBS/TX). For dual (calbindin/NeuN or calbindin/VAChT) or triple (calbindin/NeuN/VAChT) color immunofluorescence, the sections were incubated overnight at 4°C with different combinations of primary antibodies against calbindin D28K (rabbit pAb; dilution, 1:2000), NeuN (mouse mAb; 1:1000), or VAChT (goat pAb; 1:1000). Immunofluorescence was visualized with donkey anti-rabbit, anti-mouse, or anti-goat antibodies (1:50 dilutions) coupled with α methylcoumarin (AMCA), cyanine 3 (Cy3), Cy5, or FITC (Jackson ImmunoResearch, West Grove, PA). All primary and secondary antibodies were diluted in PBS/TX. Finally, after washing the excess of antibodies with PBS, the sections were coverslipped with Vectashield (Vector Laboratories, Burlingame, CA).

Confocal microscopy and image analysis. Dual Cy3 and FITC immunofluorescence and triple Cy3, FITC, and AMCA immunofluorescence were visualized with a Fluoview FX laser-scanning confocal microscope (Olympus, Tokyo, Japan), except that AMCA fluorescence was recorded with normal epifluorescence and a digital camera (Spot2; Diagnostic Instruments, Sterling Heights, MI). Triple color immunolabelings including FITC, Cy3, and Cy5 fluorochromes were imaged in a TCS confocal system (Leica, Nussloch, Germany). The proportions of calbindin-immunoreactive (IR) profiles to all small-sized NeuN-IR profiles in ventral LVII and LIX were estimated in low-magnification confocal images (10×) using ImagePro-Plus software (version 3.0.01; Media Cybernetics, Silver Spring, MD). The border between LIX and LVII was delineated by the distribution of motoneuron cell bodies (large NeuN-IR profiles). To accommodate for the progressive spinal cord growth and to minimize sampling variations, counting in ventral LVII was performed using a rectangular window, the linear dimensions of which were increased in steps of 25 μm for each successive older age group (200–275 μm width and 100–175 μm height from P1 to P15) (see Fig. 1*A*, *B*). The box was placed in ventral LVII with the lateral border aligned to the medial margin of the LIX lateral motoneuron pool and the ventral border with the ventral funiculus gray–white matter boundary. The box in LIX was placed as a lateral extension in LIX of boxes drawn in LVII at each age. Sections from 12 animals (3 per age group), with at least three sections per animal (i.e., six ventral horns), were included in the analysis. To reduce errors because of assumptions about similarities in cell body size, shape, or orientation of ventral interneurons, only nucleolus-containing IR profiles were counted. Errors caused by differential splitting of cells at the surfaces were avoided by counting only nucleoli at least 3 μm within the tissue sections. These precautions were taken to assure unbiased sampling of profiles from RCs versus other neuronal subtypes. All counts were performed in the lumbar 4 and 5 segments.

To reconstruct VAChT coverage on calbindin-IR or NeuN-IR cells, optical section stacks (step size, 0.5 μm) were obtained throughout the cell body and proximal dendrites of the neurons. Dual immunofluorescence was captured in two-channel mode with a 60× oil immersion objective (numerical aperture, 1.4) digitally zoomed 1.5×. Cross talk between channels was avoided as in previous reports (Geiman et al., 2002). Images used for figure composition were filtered (high-Gauss filter, Image Pro-Plus 4.0; Media Cybernetics) and adjusted for contrast, brightness, and dynamic resolution for best quality presentation without changing or altering the information content in the images.

Slice preparation. We recorded ventral horn interneurons from spinal cord slices obtained from 1- to 5- or 9- to 15-d-old postnatal rat pups. All animals were anesthetized (50 mg/kg pentobarbital) and decapitated, and their spinal cords were removed quickly. Dissection was in ice-cold (<4°C) sucrose artificial CSF (S-aCSF) bubbled with 95% O_2 and 5% CO_2. The S-aCSF composition was as follows (in mM): 26 $NaHCO_3$, 10 glucose, 3 KCl, 1.25 NaH_2PO_4, 2 $MgCl_2$, 2.4 $CaCl_2$, and 218 sucrose. Transverse slices from the L4–L5 segments (300–400 μm thick) were cut using an OTS-4000 tissue slicer (Electron Microscopy Sciences, Fort Washington, PA). Slices were transferred to normal oxygenated aCSF (in which sucrose was removed and 130 mM NaCl and 2 mM $CaCl_2$ were added) and incubated for 1 h at 36°C and then allowed to stabilize at room temperature (22–25°C) for at least 30 min before electrophysiological recordings. Slices were transferred into the recording chamber and perfused continuously (at a rate of 4 ml/min) with oxygenated normal aCSF.

Whole-cell recordings. Whole-cell voltage-clamp recordings were obtained from somata of visually identified ventral horn interneurons (<25 μm diameter) using an Olympus BX 50WI microscope equipped with infrared-differential interference contrast (DIC), a 40× water immersion objective, and a CCD camera (CCD-Iris; Sony, Tokyo, Japan). Preferential recording areas were ventral LVII and LIX regions containing the highest densities of immunocytochemically identified RCs (see Fig. 2*A*, *B*). Patch electrodes (2–5 MΩ resistance) contained the following (in mM): 120 CsCl, 4 NaCl, 4 $MgCl_2$, 1 Cl_2Ca, 10 HEPES, 0.2 EGTA, 3 Mg-ATP, and 0.3 GTP-Tris. In all of the experiments, 0.4% Neurobiotin (Vector Laboratories) was added to the internal solution. Only recordings with access resistance between 5 and 20 MΩ were considered acceptable for analysis. The access resistance was checked throughout the experiments, and recording was abandoned if it changed >15%. Junction potentials (usually <5 mV) were corrected after inserting the pipette into the bath. Cells were voltage clamped at −75 mV. In our recording conditions, the reversal potential for chloride currents was close to 0 mV;

Table 1. Properties of glycinergic mPSCs

	Glycinergic mPSC parameters					
	Rise time (ms)	Amplitude (pA)	Decay time (ms)	τ_{Gly} (ms)	Frequency (Hz)	Q (pC)
RCs						
P1–P5 ($n = 6$)	1.71 ± 0.23	37 ± 5	6.7 ± 0.9	6.7 ± 0.5	0.21 ± 0.06	0.44 ± 0.03
P9–P15 ($n = 6$)	0.78 ± 0.06*	124 ± 10*	4.0 ± 0.3*	3.6 ± 0.4*	0.70 ± 0.21	0.68 ± 0.07*
Non-RCs						
P1–P5 ($n = 6$)	1.79 ± 0.21	46 ± 8	7.6 ± 0.8	7.5 ± 0.8	0.47 ± 0.14	0.39 ± 0.08
P9–P15 ($n = 7$)	0.96 ± 0.13*	60 ± 5§	4.2 ± 0.2*	3.8 ± 0.2*	1.69 ± 0.63*	0.35 ± 0.04§

Values are mean ± SE. The asterisks indicate significant differences ($p < 0.05$; two-way ANOVA; Duncan's multiple range test) between age groups; the § symbols indicate significant differences between RCs and non-RCs of the same age.

thus, GABAergic and glycinergic currents were readily detected as inward currents well separated from baseline noise. Synaptic currents were recorded and low-pass bessel filtered at 5 kHz with an Axopatch 200B amplifier (Axon Instruments, Union City, CA). Data were digitized at 10 kHz and acquired using Axograph (version 4.6; Axon Instruments). For each cell, we obtained two to three segments of 5 min continuous recording of spontaneous activity under drug combinations that pharmacologically isolated the synaptic currents of interest.

To isolate miniature spontaneous synaptic currents of GABAergic and/or glycinergic origin [miniature postsynaptic currents (mPSCs)], recordings were performed in the presence of tetrodotoxin (TTX) (1 μM; Alomone Labs, Jerusalem, Israel), 6-cyano-7-nitroquinoxaline-2,3-dione (CNQX) (10 μM; Tocris Cookson, Ballwin, MO), and D-tubocurarine chloride (10 or 30 μM; Sigma, St. Louis, MO) applied by bath perfusion. Glycinergic or GABAergic mPSCs were subsequently isolated by adding either bicuculline methiodide (10 μM; Sigma) or strychnine hydrochloride (0.25 μM; Sigma) to the aCSF solution.

Data analysis. Off-line data analysis and curve fitting was performed with both pClamp 9.0 and MiniAnalysis (Synaptosoft, Decatur, GA). Events were detected by setting the threshold value for detection at three times the level of the root mean square noise (~3 pA). Therefore, the detection threshold was 8–10 pA. We routinely scrolled through detected events and visually rejected any superimposed or spuriously detected events. Peak mPSC amplitudes were measured at the absolute maximum of the currents, taking into account the noise at baseline and around the peak. Time to decay was calculated as the time from peak to 33% decay of peak amplitude. Rise times were measured between 10 and 90% of the peak. The charge transferred (in picocoulombs) was measured as the integrated area under averaged mPSCs.

Curve fitting to mPSC decay (from peak to end) was performed on averaged traces with simplex algorithm least squares exponential fitting provided by MiniAnalysis software and using single- or double-exponential equations of the form: $y = A_0 + A\,e^{(-x/\tau)}$ and $y = A_0 + A_f e^{(-x/\tau_f)} + A_s e^{(-x/\tau_s)}$, respectively. Decay phases of individual mPSCs recorded under TTX, CNQX, and D-tubocurarine chloride were fitted either by one or two exponential functions that usually resulted in events falling into one of three classes: "fast decay," "slow decay," or mixed events (see Results). The averaged glycinergic and GABAergic mPSCs in individual neurons were always best fitted by a biexponential decay. In contrast, individual and averaged mPSC decays of pharmacologically isolated glycinergic or GABAergic events were best fitted by single monoexponential curves. Although this procedure yielded good correlation fits (usually $r > 0.95$) for averaged events and many individual mPSCs, it failed in a proportion of individual events in which curve fits clearly departed from trace points ($r < 0.7$). For this reason, classification of events falling in fast-decaying, slow-decaying, and mixed categories in recordings containing mixed $GABA_A$ and glycinergic currents was aided by visual inspection of individual events in which the program failed to provide good curve fitting. These events showed fluctuations in their decay phases usually because of superimposition of other events or random baseline oscillations. The proportion of events added by visual identification of inflections in their decays were, on average (of all cells analyzed), as follows: P1–P5 RCs, 14.8% of all events; P9–P15 RCs, 4.0%; P1–P5 non-RCs, 13.4%; P9–P15 non-RCs, 1.8%. Not surprisingly, more events were added in younger cells displaying the longer decays (Tables 1-3). In a few young neurons with high frequencies of spontaneous mPSCs they represented 20–25% of all events. Using this method, we avoided underestimation of the total numbers of mPSCs for the purpose of calculating frequencies. Decay time constants of visually selected fast- and slow-only events were not significantly different from the decay constants of, respectively, glycinergic or GABAergic currents pharmacologically isolated. Mixed events were clearly identified by the presence of an inflection separating slow and fast kinetic components. We expect that any biases or errors introduced by the experimenter when estimating the proportion of different classes of events should be minimal and, in any case, smaller than the errors incurred by relying only in curve fitting of individual events by the analysis program. Two-way ANOVA and *post hoc* Duncan's multiple range tests with $p < 0.05$ were used for statistical comparisons among different ages and classes of neurons. Data were expressed as mean ± SE.

Immunohistochemical processing of recorded slices. Neurons were filled with Neurobiotin during recording. Spinal cord slices containing Neurobiotin-filled neurons were fixed in 4% paraformaldehyde for 30 min and then stored at 4°C in PBS. Immunohistochemistry was performed in the thick slices used for recording. To facilitate penetration of antibodies, tissue sections were dehydrated and rehydrated through a graded series of alcohols and xylene. Slices were then washed in PBS, blocked with NHS (1:10 in PBS/0.2% TX), and immersed free-floating in primary antisera against VAChT (diluted 1:1000 in PBS/TX; the concentration of Triton X-100 was adjusted in these thick slices to 0.3% to favor penetration). Incubations were performed overnight at room temperature and under agitation. Thereafter, slices were washed and incubated for 2 h in streptavidin–Cy3- and FITC-coupled donkey anti-goat antibodies diluted in PBS/TX (1:50 dilutions; Jackson ImmunoResearch). Finally, slices were mounted on glass slides and coverslipped with Vectashield (Vector Laboratories).

Neuronal localization (Cy3–Neurobiotin labeling) was first visualized under epi-fluorescence with an Olympus BX60 microscope. Low-magnification (10×) and high-magnification (40×) images were captured with a digital color camera (Spot2 camera; Diagnostic Instruments) to plot the location of the neuron somata and record major morphological properties of dendrites and axon trajectories. VAChT immunoreactivity in low-magnification images pointed to the location of motoneurons and LIX. The cell body locations of all neurons included in the study ($n = 41$ at P1–P5 and $n = 51$ at P9–P14) were plotted in relation to the section outline, the ventral horn gray matter, and the location of LIX. The average representation of these locations is shown in Figure 2*B*. Finally, the density of VAChT-IR contacts was analyzed with confocal microscopy. Labeled neurons (Cy3) and VAChT immunofluorescence (FITC) were scanned in two-channel mode in an Olympus Fluoview FX confocal microscope. Cell morphology and VAChT-IR bouton contacts were reconstructed from stacks of optical sections (1 μm step size) obtained at 60×2 magnification. The recorded neurons were classified into RC and non-RC groups according to the density of VAChT-IR terminals contacting the somatodendritic surfaces, as well as the location of the cell body, extension of the dendrites, and the presence of axon collaterals in the ipsilateral motoneuron pool (frequently containing synaptic-like varicosities). The characteristics of GABAergic and glycinergic synaptic currents were compared throughout postnatal development between both groups of neurons.

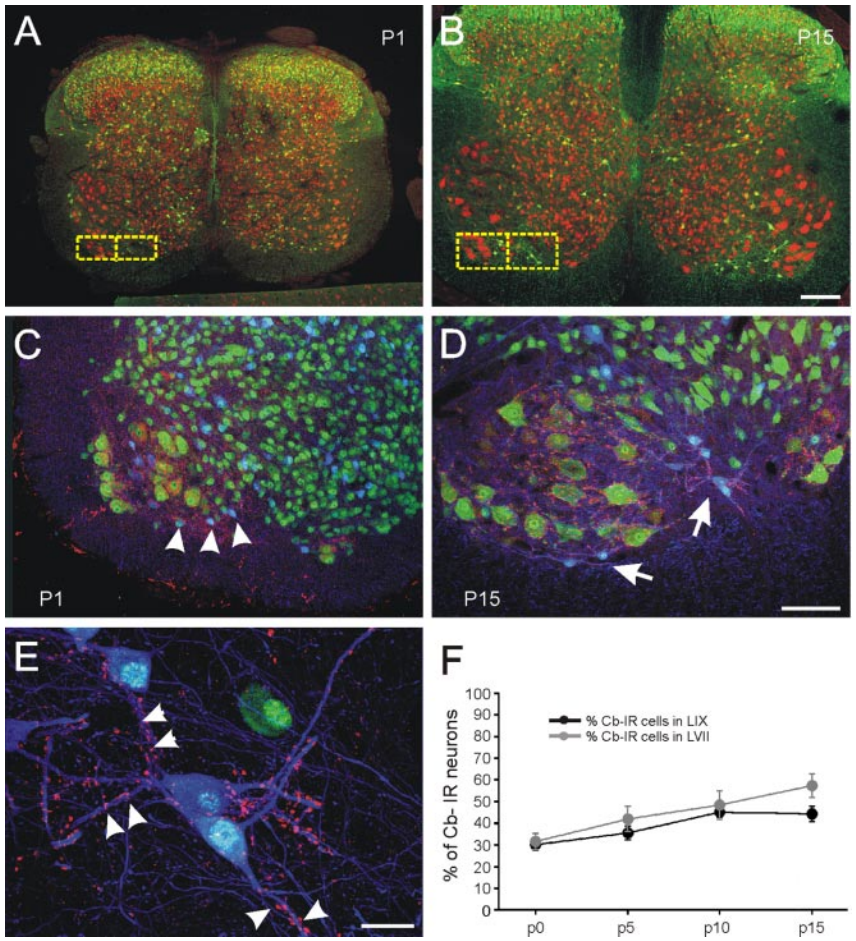

Figure 1. Distribution of immunohistochemically defined RCs in the ventral horn. ***A***, ***B***, Low-magnification confocal images showing the distribution of calbindin-IR (FITC; green) and NeuN-IR (Cy3; red) neurons in the spinal cord at P1 (***A***) and P15 (***B***). The RC region was identifiable at both ages in ventral LVII and LIX and contains a relatively high density of calbindin-IR neurons. The boxes indicate the placement and dimensions of the areas used to estimate neuronal percentages in ventral LVII and LIX. The percentage of calbindin-IR neurons to all other neurons was estimated inside these boxes. ***C***, ***D***, Triple immunofluorescence for calbindin (Cy5; blue), NeuN (FITC; green), and VAChT (Cy3; red) in the ventral horn of P1 and P15 rat spinal cords. Neuronal density in ventral LVII was higher at P1. The distribution of calbindin-IR neurons is noted with arrowheads at P1 (***C***) and with arrows at P15 (***D***). VAChT immunoreactivity was strong in C-boutons surrounding LIX motoneurons and in varicosities contacting small-sized calbindin-IR neurons located in ventral LVII or LIX. The area pointed to in ***D*** is shown at higher magnification in ***E***. ***E***, The density of VAChT-IR contacts (Cy3; red) was higher on dendrites (arrowheads) and somata of calbindin-IR neurons (Cy5; blue) compared with NeuN-IR (non-calbindin-IR; FITC; green) neurons. ***F***, Percentages of calbindin (Cb)-IR neurons (RCs) to all NeuN-IR neurons of small size (i.e., interneurons; large-sized NeuN-IR motoneurons were excluded from the counts) gradually increase with age in ventral LVII (gray circles) and LIX (filled circles). Scale bars: (in ***B***) ***A***, ***B***, 200 μm; (in ***D***) ***C***, ***D***, 100 μm; ***E***, 20 μm.

Results

Targeting and identification of recorded neurons as RCs

RCs are characterized by monosynaptic cholinergic inputs from motor axon collaterals, strong calbindin expression, large gephyrin clusters on their proximal somatodendritic membranes, and preferential location of lower lumbar segments in ventral LVII and ventral LIX (Eccles et al., 1954; Jankowska and Lindstrom, 1971; Fyffe, 1990; Ardvisson et al., 1992; Alvarez et al., 1997, 1999; Carr et al., 1998). Two previous studies in spinal cord slices used stimulation of motor axons as search stimulus to identify and record RCs (Oleskevich et al., 1999; Dourado and Sargent, 2002). In both studies, ventral root cholinergic monosynaptic inputs were identified in <10% of recorded neurons. This low yield could have resulted from targeting ventral horn regions with low densities of RCs and perhaps also from motor axon damage during slicing. To overcome these problems, we determined anatomically the optimal sampling sites in the neonatal spinal cord and tested several properties for RC *post hoc* histochemical identification.

Intense calbindin immunoreactivity is a distinctive feature of RCs (Ardvisson et al., 1992; Carr et al., 1998; Geiman et al., 2000). Ventral horn neurons with intense calbindin immunoreactivity are mostly located in ventral LIX and LVII (Fig. 1*A*,*B*), in a region corresponding to the adult RC area (Thomas and Wilson, 1965; Jankowska and Lindstrom, 1971; Fyffe, 1990). The proportion of calbindin-IR neurons to all NeuN-IR small-sized neurons increased during postnatal development from 30.1 ± 2.6% (P1–P5; mean ± SE) to 44.3 ± 3.6% (P10–P15) in ventral LVII and from 31.6 ± 3.8% to 57.3 ± 5.4% in ventral LIX (Fig. 1*F*) (see Materials and Methods for a description of the boxed regions of interest that were analyzed). At the same time, expansion of the neuropil reduced neuronal density from P1 to P15, particularly in ventral LVII (Fig. 1, compare *C*, *D*). In conclusion, sampling in the low cell density region shown in Figure 2*A* should result in a 30–60% chance of recording from an RC. This region appears darker with DIC optics because of the increased density of myelinated axons, likely motor axons, crossing this area.

This distinctive regional distribution is important for targeting recordings to RCs, but it is insufficient to identify this neuronal phenotype. Therefore, we investigated other features that could permit RC identification. Adult calbindin-IR RCs display high densities of cholinergic contacts on their dendrites (Alvarez et al., 1999). Similarly, neonatal calbindin-IR RCs received higher densities of VAChT-IR contacts than other NeuN-IR neurons (Fig. 1*C–E*). Two other features of adult RCs, large gephyrin clusters and calbindin immunoreactivity, were inadequate for RC characterization in the present study. Gephyrin-IR clusters on RCs undergo postnatal maturation (Geiman et al., 2000), and in neonates they are not different from gephyrin-IR clusters on other neurons (data not shown). On the other hand, calbindin immunoreactivity in recorded neurons was weaker and more difficult to detect than in non-recorded cells. Possibly, calbindin dilution into recording pipettes significantly lowers calbindin immunoreactivity in neurons recorded in whole-cell mode.

Neurons selected for recording were visualized with DIC optics in the target region. Thereafter, *post hoc* immunohistochemical confirmation of a high density of VAChT-IR contacts on Neurobiotin-filled neurons was a necessary condition for RC classification (Fig. 2*C*,*D*); 27.5% (60 of 218) of intracellularly recorded and stained cells were classified as RCs in our target population. Only neurons with good quality recordings (>25 min of stable recordings at constant low series resistance) and

intracellular staining and in sections with successful VAChT immunolabeling were analyzed. VAChT immunolabeling of C terminals on neighboring motoneurons (Alvarez et al., 1999) was used as internal control of immunolabeling quality. The locations of neurons analyzed are shown in Figure 2*B*. We analyzed 20 neurons identified as RCs at each age (P1–P5 and P9–P15). All RCs were preferentially located within the ventralmost 200 μm of LVII and LIX. RC axons were directed toward ipsilateral motor pools, and sometimes varicosities were observed in LIX. The dendrites of RCs formed small arbors, mostly restricted to the RC area. Non-RC interneurons were more disperse in the ventral horn, occasionally distant from the motoneuron pools, and their morphological features were very variable. Axons recovered from non-RCs projected toward ipsilateral LIX motoneurons pools, crossed the midline into the contralateral spinal cord, or coursed toward the lateral funiculus. Some dendritic arborizations in this cell group were large and widespread, whereas others had restricted distributions. Thus, non-RCs likely comprise several neuronal subtypes. We analyzed 21 non-RCs at P1–P5 and 31 at P9–P15.

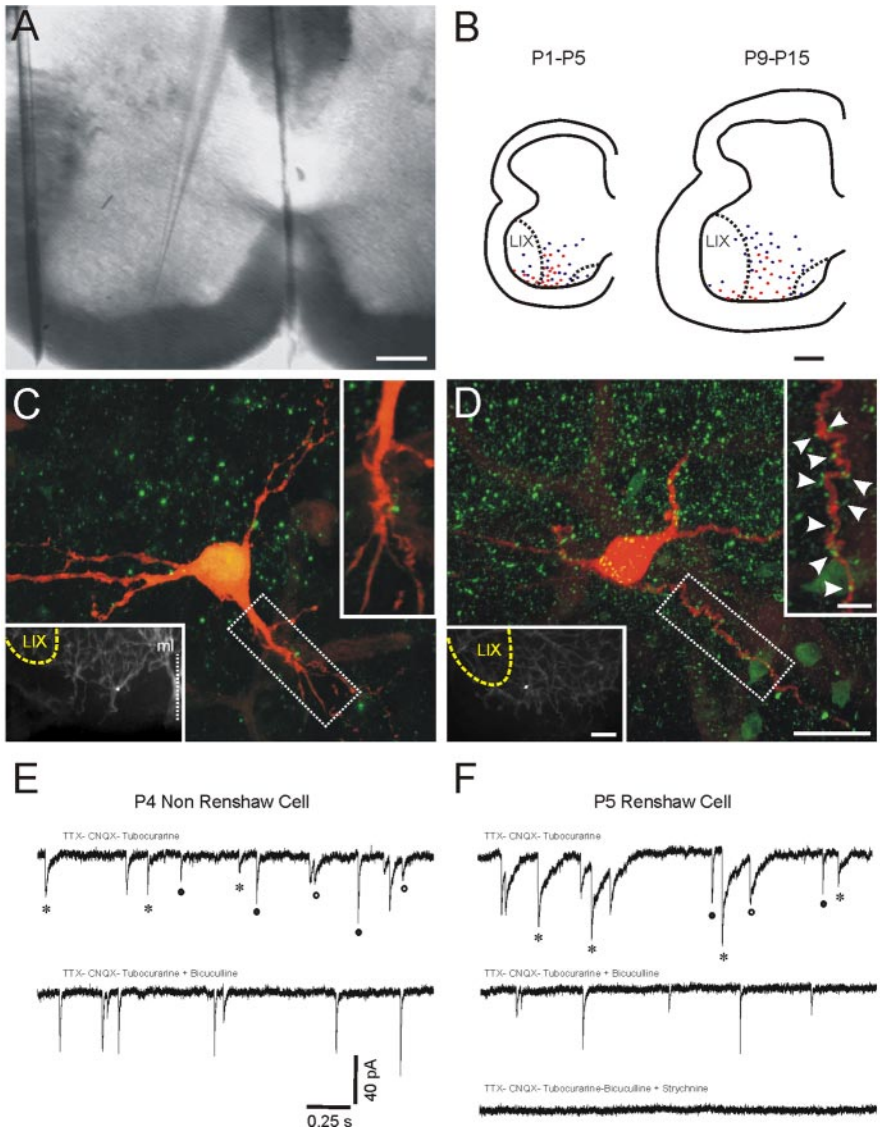

Figure 2. Immunohistochemical identification and recording from ventral horn interneurons. ***A***, Representative image of a P12 rat spinal cord slice through the lower lumbar region. A patch pipette is visible in the image and points to the area targeted for recordings containing the highest densities of RCs. This area appears slightly darker under infrared-DIC optics because of its high content in myelinated motor axons. ***B***, Schematic maps showing the location of interneurons recorded at P1–P5 (left) and P9–P15 (right). Red dots, RCs; blue dots, non-RCs. The dashed lines delineate lateral and medial motoneuron pools (LIX). ***C***, ***D***, Superimposition of confocal optical sections reconstructing VAChT-IR coverage (FITC; green) on two Neurobiotin-filled (Cy3; red) ventral horn interneurons at P4 and P5 and respectively classified as a non-RC (***C***) and an RC (***D***). The bottom left insets are single optical sections indicating localization of each neuron (Cy3; black and white images) relative to LIX and midline (ml; dotted line). The top right insets are higher-magnification images of boxed dendrites in ***C*** and ***D***. Note the dense coverage by VAChT-IR varicosities on the RC dendrite shown in ***D***. ***E***, ***F***, GABA and glycine mPSCs recorded in the cells shown in ***C*** and ***D***. Neurons were voltage clamped at −75 mV, and mPSCs were isolated with TTX (1 μM), CNQX (10 μM), and D-tubocurarine (30 μM). The reversal potential for Cl^--mediated currents was close to 0 mV. Neurons exhibited fast-decaying (filled circles), slow-decaying (open circles), and dual-component (asterisks) mIPSCs (top traces). Slow and mixed events had longer durations in RCs. Glycinergic or GABAergic mPSCs were subsequently isolated by adding bicuculline (10 μM; ***E***, ***F***, middle traces) or strychnine (0.25 μM) (see Fig. 5) to the aCSF. Isolated glycinergic currents were blocked with strychnine (example shown in ***F***), and isolated GABAergic currents were abolished with bicuculline. Scale bars: ***A***, ***B***, 200 μm; (in ***D***) ***C***, ***D***, 20 μm; ***C***, ***D***, left inset, 100 μm; ***C***, ***D***, color inset, 5 μm.

Differential maturation patterns of GABAergic/glycinergic mPSCs in ventral horn interneurons

We first compared all "inhibitory" mPSCs isolated with TTX, CNQX, and D-tubocarine in RCs ($n = 7$ at P1–P5 and $n = 7$ at P9–P15) and non-RCs ($n = 9$ at P1–P5 and $n = 8$ at P9–P15). These mPSC events are mixtures of GABAergic and glycinergic events, hereafter called $mPSCs_{GABA/Gly}$, and were blocked by 10 μM bicuculline and 0.2–1 μM strychnine (Fig. 2*E*,*F*).

In both cell types, some events decayed rapidly (decay time, ≤15 ms), others slowly (decay time, >15 ms), and some were mixed (events with fast and slow components, frequently separated by inflections in their decays). RCs always showed a significant population of mPSCs with very slow decays. These were infrequent in non-RCs. This difference was evident at early stages (Fig. 2*E*,*F*) and increased with age (Fig. 3*A*,*B*). At late postnatal ages, few $mPSC_{GABA/Gly}$ events (3.76%) were longer than 20 ms in non-RCs (Fig. 3*A*,*C*,*E*); these were more common in RCs (16.6%) (Fig. 3*B*,*D*,*F*). Rise time versus decay time plots showed a compression of the decay time range in non-RCs during postnatal development (Fig. 3*C*). On the contrary, $mPSCs_{GABA/Gly}$ in RCs of ages P1–P5 and P9–P15 showed similar wide ranges of decay times (Fig. 3*D*). Thus, decay time cumulative distributions shifted to the left in non-RCs, indicating faster decay kinetics in older animals (Fig. 3*E*), whereas the cumulative curve from P9–P15 RCs was slightly displaced to the left for faster events and to the right for slower events (Fig. 3*F*). It is unlikely that electrotonic filtering contributed to differences in decay between both cell types. First, $mPSC_{GABA/Gly}$ mean rise times in P9–P10 RCs and non-RCs were similar (1.5 ± 0.2 vs 1.3 ± 0.1 ms, respectively; $p = 0.42$; two-way ANOVA; Duncan's test). Second, correlations between rise and decay times were never

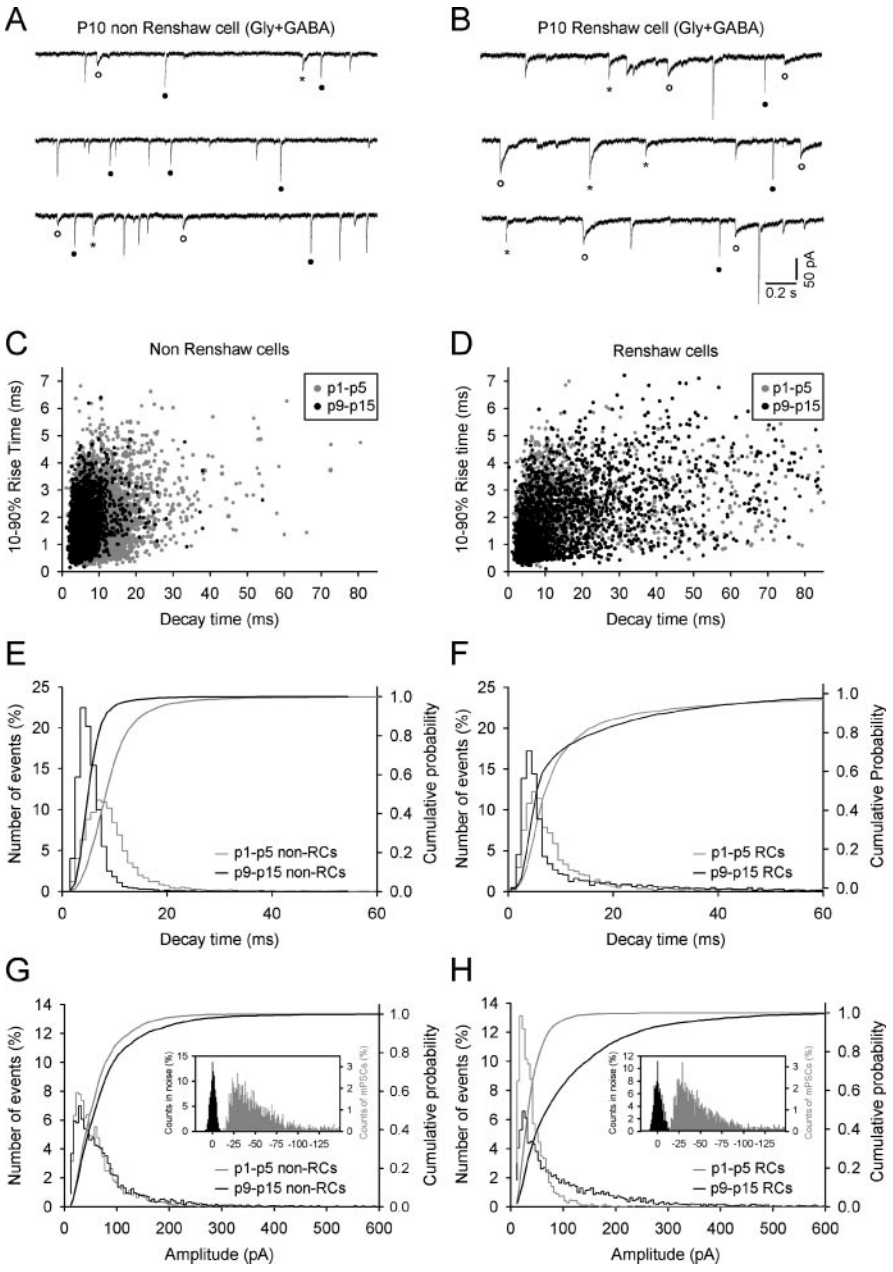

Figure 3. Maturation of $mPSC_{GABA/Gly}$. ***A***, ***B***, mPSCs recorded in presence of TTX, CNQX, and D-tubocurarine from a P10 non-RC (***A***) and RC (***B***). $V_{hold} = -75$ mV. Fast-decaying (filled circles), slow-decaying (open circles), and mixed (asterisks) events could be distinguished in both neurons. Dual and slow-decaying components were longer and more frequent in RCs. ***C***, ***D***, Relationships between 10–90% rise time and decay time in non-RCs (***C***) and RCs (***D***) recorded at P1–P5 (gray dots) or P9–P15 (black dots). Data obtained from nine non-RCs (***C***; $n = 4766$ events) and seven RCs (***D***; $n = 2863$ events) recorded between P1 and P5 and from eight non-RCs (***C***; $n = 3801$ events) and seven RCs (***D***; $n = 4056$ events) recorded from P9–P15 postnatal rats are shown. The range of decay times was shortened with development in non-RCs but not in RCs. There was no correlation between rise and decay times ($r < 0.2$). ***E***, ***F***, Distribution histograms and cumulative probability plots of decay times for the same events shown in ***C*** and ***D***. Bin width, 1 ms. ***G***, ***H***, Same as in ***E*** and ***F*** but for mPSC peak amplitudes. The event amplitude in RCs increased with age (***H***) but not in non-RCs (***G***). RC amplitude distribution histograms become more skewed to higher values at late postnatal ages, and the corresponding cumulative probability curve shifted to the right. In comparison, non-RCs show little differences in peak amplitude. Bin widths, 5 pA. The insets show examples of mPSC amplitude distributions (gray bars) in two individual neurons of each class (at P2–P3) and the distribution of the recording noise (black bars). Smaller bin widths (1 pA) were used for comparisons of noise with detected mPSCs. The scale in the *x*-axis is shown up to 150 pA to show more clearly the separation between noise and detected events. In our recording conditions, detected mPSCs were well separated from noise.

found ($r < 0.2$) (Fig. 3*C*,*D*). Finally, the dendritic arbors of non-RCs (with shorter decay times) were usually larger than in RCs, and RCs have less distal inhibitory synapses than non-RCs (Alvarez et al., 1997).

Peak amplitudes of $mPSCs_{GABA/Gly}$ were also differentially regulated during postnatal development in each neuronal type. The mean peak $mPSC_{GABA/Gly}$ amplitude increased by 121.3% [100 × value(P9–P15) − value(P1–P5)/value(P1–P5)] in the RC group ($p < 0.05$; two-way ANOVA; Duncan's test). In contrast, the average peak amplitude increase in non-RCs was moderate and did not reach statistical significance (61.2%; $p = 0.07$). Cumulative probability plots of peak $mPSC_{GABA/Gly}$ amplitudes shifted to the right with development in both RCs and non-RCs. The magnitude of change was much greater for RCs (Fig. 3*G*,*H*), and peak amplitude distribution histograms in P9–P15 RCs showed strong skews toward high-amplitude events.

In addition, we observed developmental changes in frequency, but these are best reported below, following descriptions of individual and mixed GABA/glycine unitary events.

Glycinergic mPSC development

To analyze the specific neurotransmitter components of these inhibitory synaptic currents, we first isolated pharmacologically glycinergic mPSCs (called $mPSCs_{Gly}$) by blocking glutamatergic (CNQX), nicotinic (D-tubocurarine), and $GABA_A$ (bicuculline) receptors. At early postnatal times, $mPSCs_{Gly}$ were similar in both cell types (Fig. 4*A*,*B*, top traces). Mean peak amplitude, 10–90% rise time, decay time, and time constant (τ_{gly}) were not significantly different between both cell types ($p \geq 0.05$; two-way ANOVA; Duncan's test) (Table 1). During development, $mPSC_{Gly}$ decays became faster in both cell types (Fig. 4*A*–*F*; *C*,*D*, insets; Table 1). Rise time versus decay time plots (Fig. 4*C*,*D*) and distribution histograms (Fig. 4*E*,*F*) revealed a shortening in the range of decays, the mean values of which for RCs and non-RCs were, respectively, 1.69 and 1.82 times faster to those in P1–P5 neurons (Table 1). Common kinetic changes in pharmacologically isolated $mPSCs_{Gly}$ probably reflect similar maturation of postsynaptic glycine receptor functional properties in both cell types. In contrast, $mPSC_{Gly}$ amplitudes matured differently in RCs and non-RCs (Fig. 4*G*,*H*; Table 1). P9–P15 RCs exhibited a large increase (230.4%) in mean $mPSC_{Gly}$ peak amplitude, relative to P1–P5 RCs. In contrast, the smaller increase (31%) in mean peak amplitude in non-RCs did not reach statistical significance ($p = 0.2$; two-way ANOVA; Duncan's test). Consequently, non-RC $mPSC_{Gly}$ amplitude distribution histograms of different ages essentially overlapped, and only a very small shift was noted

in their cumulative probability functions (Fig. 4*G*). In contrast, amplitude distributions from P9–P15 RC $mPSCs_{Gly}$ were mostly skewed toward higher values, and their probability functions significantly shifted to the right (Fig. 4*H*). Thus, whereas $mPSCs_{Gly}$ with amplitudes >100 pA were infrequent in RCs at early ages (4.5% of all events) and in non-RCs at early and late postnatal ages (11.0 and 14.8%, respectively), events >100 pA comprised nearly 50% of all $mPSCs_{Gly}$ in P9–P15 RCs.

The frequency of pharmacologically isolated glycinergic events increased more than twofold from early to late postnatal ages in both RCs and non-RCs (see Fig. 6*A3*, Table 1). Event frequencies were always higher in non-RCs of all ages. This observation parallels morphological findings indicating the presence of 5–15 small independent active zones per synapse on non-RCs compared with fewer numbers of larger active zones in inhibitory synapses contacting adult RCs (Alvarez et al., 1997).

GABAergic mPSC development

In the ventral spinal cord, spontaneous miniature GABAergic synaptic events ($mPSCs_{GABA}$) are generally downregulated in frequency and amplitude, and their duration is shortened during postnatal development (Gao et al., 2001). However, significant numbers of bicuculline-sensitive mPSCs with remarkably slow kinetics persist in mature RCs (Fig. 3). To analyze their postnatal development, $mPSCs_{GABA}$ were pharmacologically isolated in the presence of 0.25 μM strychnine added to the CNQX, D-tubocurarine, and TTX mixture (Fig. 5*A*,*B*). Pharmacologically isolated GABAergic mPSCs recorded from non-RCs ($n = 8$) and RCs ($n = 6$) at P1–P5 were similar in 10–90% rise time and peak amplitude ($p > 0.05$; two-way ANOVA; Duncan's test) (Fig. 5*G*,*H*; Table 2). However, mean decay time and τ_{GABA} of $mPSCs_{GABA}$ in neonatal RCs was 2.1 times longer than in non-RCs ($p < 0.05$; two-way ANOVA; Duncan's test) (Fig. 5*A–F*, Table 2).

Differences in pharmacologically isolated $mPSCs_{GABA}$ between both cell types increased with development (Fig. 5*A–H*). The average decay times and τ_{GABA} of $mPSCs_{GABA}$ were shortened in P9–P15 non-RCs, becoming nearly threefold faster than those measured in RCs of similar age (Table 2). Rise time versus decay time plots, distribution histograms, or cumulative probability curves were compressed or shifted toward shorter values in P9–P15 non-RCs. In contrast, their ranges essentially overlapped in RCs from both ages (Fig. 5*C–F*). Nevertheless, the averaged τ_{GABA} suggested an acceleration of $mPSC_{GABA}$ decay kinetics in RCs with development ($p < 0.05$; two-way ANOVA; Duncan's test) (Table 2). Mean peak amplitudes significantly increased by 45.1% in RCs ($p < 0.05$; two-way ANOVA; Duncan's test), while

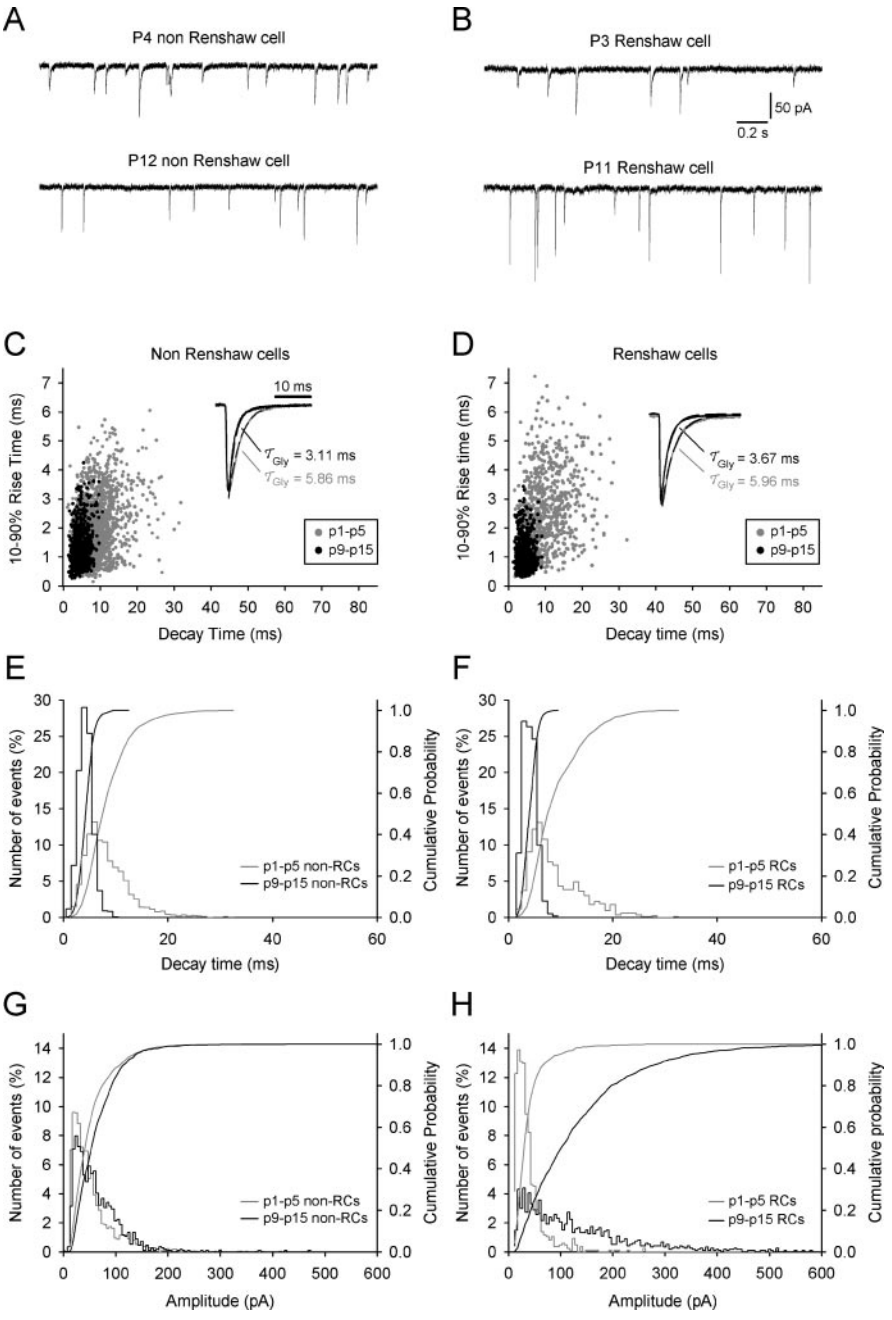

Figure 4. Development of glycinergic mPSCs. ***A***, ***B***, Glycine-mediated mPSCs recorded in the presence of bicuculline (10 μM) from non-RCs (***A***) and RCs (***B***) of different ages. Glycinergic mIPSCs became faster decaying with age in RCs and non-RCs and significantly larger in amplitude in RCs only. ***C***, ***D***, Relationships between 10–90% rise time and decay time of individual glycinergic mPSCs recorded from 10 non-RCs [***C***; 6 neurons between P1 and P5 (gray dots; $n = 2259$ events) and 4 neurons between P9 and P15 (black dots; $n = 1118$ events)] and 8 RCs [***D***; 4 neurons between P1 and P5 (gray dots; $n = 1113$ events) and 4 neurons between P9 and P15 (black dots; $n = 1209$ events)]. The insets illustrate averaged synaptic currents scaled to peak at early (P1–P5; gray traces) or late (P9–P15; black traces) postnatal ages in non-RCs (***C***) and RCs (***D***). A single exponential best fit the decay of each of these averages. Estimated values for time constants (τ_{gly}) are indicated. ***E***, ***F***, Distribution histograms and cumulative probability functions of decay times for the individual events plotted in ***C*** and ***D***. The range of decay times was similarly shortened with development in both neuronal types. Bin widths, 1 ms. ***G***, ***H***, As in ***E*** and ***F***, but for glycinergic mPSC amplitudes. Event amplitude distribution was unchanged in non-RCs with development. In contrast, mature RCs (P9–P15) show a cumulative probability function significantly shifted to the right, and the amplitude distribution histogram significantly skewed toward high-amplitude values compared with neonatal RCs (P1–P5). Bin widths, 5 pA.

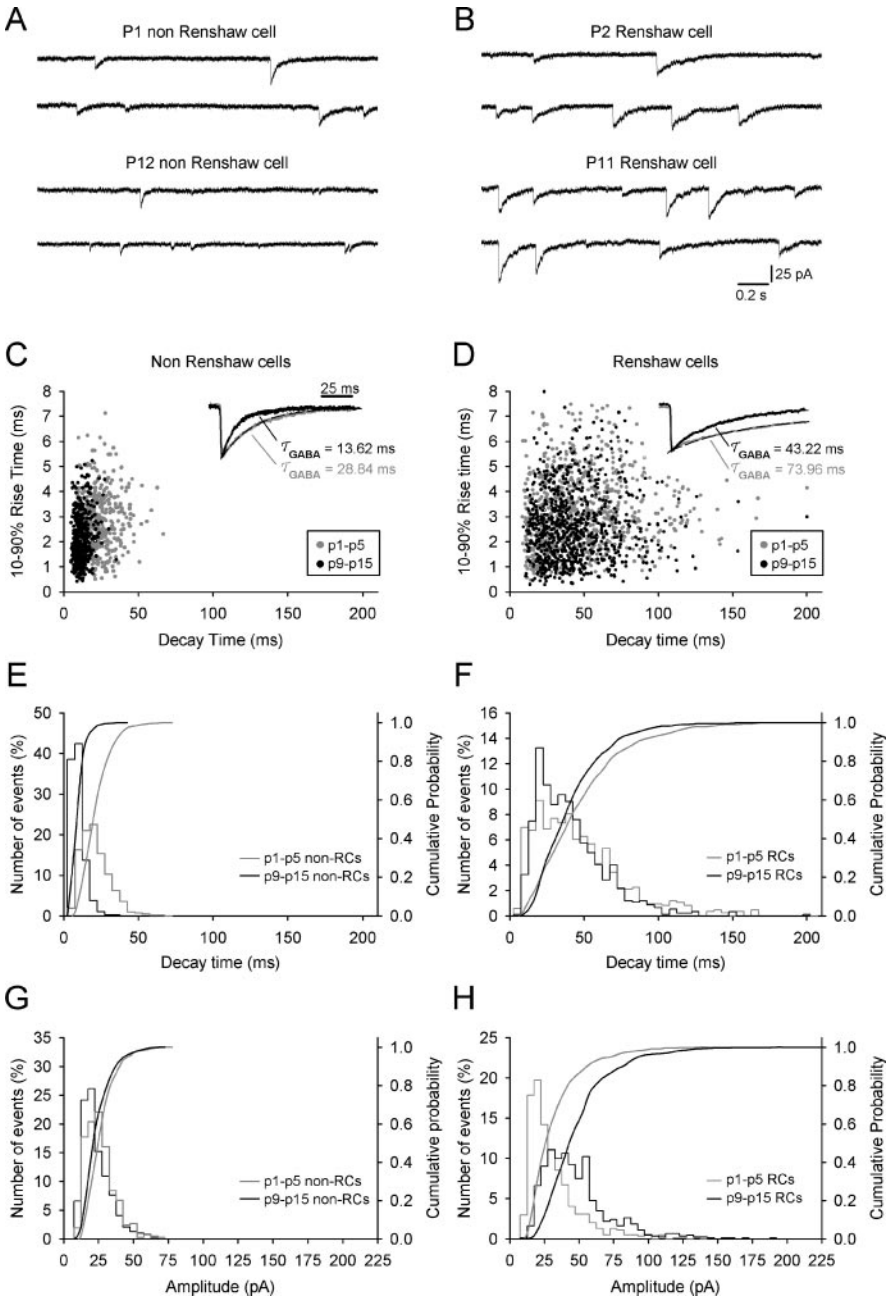

Figure 5. Development of GABAergic mPSCs. ***A***, ***B***, Representative current traces illustrating GABAergic mPSCs from non-RCs (***A***) and RCs (***B***) recorded at the ages indicated and in the presence of strychnine (0.25 μM). GABAergic mPSCs became faster decaying with age in both neuronal cell types. Mature RCs display more events with slow decays and large peak amplitudes compared with non-RCs. ***C***, ***D***, Ten to 90% rise time to decay time plots obtained from 13 non-RCs [***C***; 6 recorded between P1 and P5 (gray dots; $n = 424$ events) and 7 between P9 and P15 (black dots; $n = 394$ events)] and 12 RCs [***D***; 6 recorded between P1 and P5 (gray dots; $n = 853$ events) and 6 between P9 and P15 (black dots; $n = 928$ events)]. GABAergic mPSCs recorded from RCs were slower at all ages, and their range was severalfold wider relative to non-RCs. No correlation between the 10–90% rise time and decay time was found ($r < 0.2$). The insets illustrate average synaptic currents at early (P1–P5; gray traces) or late (P9–P15; black traces) postnatal ages scaled to peak. The decays of each of these averages were best fitted by a single exponential, and the estimated values for the time constants (τ_{GABA}) are indicated. ***E***, ***F***, Distribution histograms and cumulative probability functions of decay time for the data plotted in ***C*** and ***D***, respectively. Note that mPSC decays were accelerated in both groups with age, although the magnitude of change was much smaller for RCs. Bin width, 5 ms. ***G***, ***H***, Same as in ***E*** and ***F*** but for GABAergic mPSC amplitudes. Amplitude distribution histograms and cumulative probability plots of GABAergic mPSCs significantly shifted in older ages toward larger amplitudes in RCs but not in non-RCs. Bin widths, 5 pA.

showing a small and nonsignificant decline in non-RCs ($p = 0.27$) (Table 2).

Together, these results suggest significant differences in the functional development of inhibitory synaptic currents in RCs compared with non-RC interneurons (Fig. 6).

Postnatal development of glycine–GABA mixed mPSCs

The characteristics of inhibitory currents in RCs and non-RCs are also influenced by the amount of cotransmission between GABA and glycine. We analyzed cotransmission in both cell types by studying the characteristics of dual-component mPSCs from recordings obtained in the absence of bicuculline and strychnine, as those shown in Figures 2 and 3. According to the characteristics of pharmacologically isolated glycinergic and GABAergic mPSCs, we characterized three types of events based on their decay kinetics and developmental maturation (Fig. 7*A*): fast (≤15 ms at P1–P5 and ≤10 ms at P9–P15), slow (>15 ms at P1–P5 and >10 ms at P9–P15), and mixed (with an inflection separating fast and slow components). Decay parameters were estimated from decay phases best fitted to monoexponential or biexponential curves ($r > 0.9$ in ~80–95% fits in different cell groups). However, a population of mPSCs with long decays sometimes displayed superimposed events or other noise fluctuations that prevented good fits ($r < 0.7$). To avoid underestimation of the number of events in each category, clear mPSCs with random fluctuations in their decays were classified as fast, slow, or mixed by visual inspection and were added to the populations of mPSCs classified by curve fitting. Visually classified events are a small proportion of all of the mPSCs analyzed in each cell group (P1–P5 RCs, 14.8% of all events; P9–P15 RCs, 4.0%; P1–P5 non-RCs, 13.4%; P9–P15, non-RCs, 1.8%). Decay time constants of averaged single fast and slow mPSCs selected in this way were very similar to pharmacologically isolated glycinergic and GABAergic currents in each neuronal subgroup ($p \geq 0.1$; two-way ANOVA). Moreover, the decay constants of fast (τ_f) and slow (τ_S) components of biexponentially decaying events coincided with those obtained from single "fast" and "slow" mPSCs (Fig. 7*A*, Table 3).

The relative percentage of fast events increased significantly from early to late postnatal ages (Fig. 7*B*,*C*) in non-RCs (from 41.9 to 77.5%) and RCs (from 26.7 to 56.3%), in parallel to the developmental increase in the frequency of glycinergic mPSCs in both cell types (Fig. 6*A*3). Higher percentage values of fast mPSCs in non-RCs relative to RCs result from greater numbers of $mPSCs_{Gly}$ and a lower frequency of $mPSCs_{GABA}$ in non-RCs. The fraction of slow-decaying

Table 2. Properties of GABAergic mPSCs

	GABAergic mPSC parameters					
	Rise time (ms)	Amplitude (pA)	Decay time (ms)	τ_{GABA} (ms)	Frequency (Hz)	Q (pC)
RCs						
P1–P5 ($n = 6$)	2.9 ± 0.2	30 ± 3	47.8 ± 4.6	58.7 ± 5.1	0.20 ± 0.05	1.98 ± 0.74
P9–P15 ($n = 9$)	2.0 ± 0.3*	43 ± 5*	36.3 ± 3.6*	43.2 ± 4.4*	0.22 ± 0.04	1.82 ± 0.19
Non-RCs						
P1–P5 ($n = 8$)	1.8 ± 0.2	28 ± 2	22.8 ± 1.6§	27.2 ± 1.83§	0.21 ± 0.06	0.95 ± 0.07§
P9–P15 ($n = 9$)	1.0 ± 0.1*	24 ± 2§	12.2 ± 1.9*§	14.4 ± 0.8*§	0.07 ± 0.02*§	0.49 ± 0.04*§

Values are mean ± SE. The asterisks indicate significant differences ($p < 0.05$; two-way ANOVA; Duncan's multiple range test) between age groups; the § symbols indicate significant differences between RCs and non-RCs of the same age.

events was significantly reduced with age in non-RCs, whereas it remained unchanged in RCs. Finally, the percentage of mixed mPSCs decreased in both neuronal types, although to a larger extent in non-RCs (Fig. 7*B*,*C*). The reduction in the number of mixed events in RCs probably derives from the increased frequency of pure fast glycinergic events. Finally, the downregulation of GABAergic currents in non-RCs contributes to reduce further the incidence of dual mPSCs in these neurons compared with RCs.

To further analyze the contribution of fast (likely glycinergic) and slow (likely GABAergic) components to mixed events in RCs and non-RCs, we estimated the relative contribution to absolute peak amplitudes in mixed mPSCs of the fast and slow components (A_f, A_s) (Fig. 7*D*, Table 3). A_f and A_s were calculated from the parameters of decay curve fittings using the biexponential formula $y = A_0 + A_f e^{(-x/\tau f)} + A_s e^{(-x/\tau s)}$. As indicated by the A_f/A_s ratios in Figure 7*D*, the relative contribution of the fast component was similar in RCs and non-RCs at early postnatal ages, accounting for ~60% of the total peak amplitude (Table 3). The relative contribution of fast versus slow components was similar in non-RCs of different ages, whereas A_f/A_s ratios were significantly increased in RCs at later postnatal ages (Fig. 7*D*) ($p < 0.05$; two-way ANOVA; Duncan's test). In conclusion, GABAergic mPSCs and GABAergic components in mixed mPSCs were maintained during development to a larger extent in RCs compared with non-RCs. Thus, GABAergic currents are responsible for the retention in RCs of mixed events with slow decays during development, but their contribution to peak amplitudes is reduced in older ages because the large increase in the fast glycinergic currents.

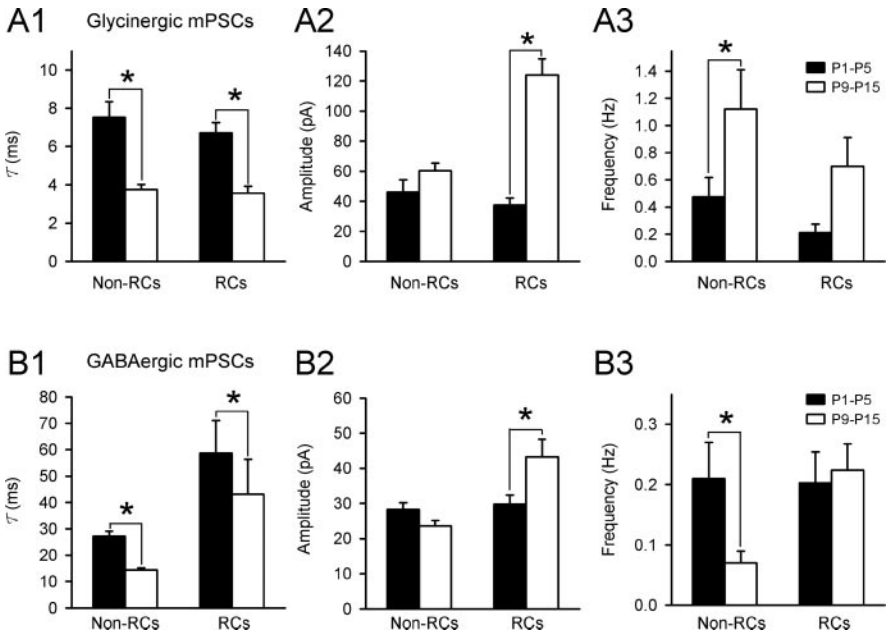

Figure 6. Analysis of averaged developmental changes in glycinergic and GABAergic mPSCs. ***A1–A3***, Averaged values of the decay time constant τ (***A1***), peak amplitude (***A2***), and frequency (***A3***) for glycinergic mPSCs in non-RCs and RCs recorded at early (P1–P5; ■) or late (P9–P15; □) postnatal ages. ***B1–B3***, Same as ***A1–A3*** but for GABAergic mPSCs. Glycinergic mPSCs were faster and more frequent with age in both non-RCs and RCs. Glycinergic mPSC peak amplitude increased dramatically in RCs but not in non-RCs. GABAergic mPSCs were unchanged in frequency, slightly faster in decay, and larger in amplitude with development in RCs, whereas they were accelerated and downregulated in peak amplitude and frequency in non-RCs. The asterisks indicate significant differences between both age groups with $p < 0.05$ (two-way ANOVA; *post hoc* Duncan's test). Data were obtained from cells in Tables 1 and 2 and are expressed as mean ± SE.

Charge transfer of GABA/glycine mPSCs in mature ventral horn interneurons

Although GABAergic components might contribute to peak amplitude less than glycinergic components, their long time courses suggest strong contributions to the total inhibitory synaptic current. We calculated the total charge transferred by glycinergic and GABAergic components in single and dual mPSCs in RCs and non-RCs recorded from P9–P15 animals. Absolute charge transfer associated with glycinergic, GABAergic, or mixed currents recorded from RCs was always larger than for non-RCs [Fig. 8, filled circles (RC), open circles (non-RCs); Tables 1–3). Both peak amplitudes and time courses contributed to increase charge transfer, but the relative contributions of each parameter was different for GABA or glycine mPSCs. Correlations between charge and peak amplitude or decay constant of glycinergic, GABAergic, or dual mPSCs suggest that absolute charge transfer is better related with peak amplitude, but not with decay time, in fast glycinergic mPSCs and with both decay time and peak amplitude in slow GABAergic mPSCs (Fig. 8*A1–B2*). As a result, in mixed mPSCs, both peak amplitude (dominated by the fast glycinergic current) and time course (dominated by the second decay from the slower GABAergic currents) are both well correlated with peak amplitude (Fig. 8*C1–C3*).

Discussion

Inhibitory synapses on mature RCs are characterized by larger peak amplitudes, slower decays, and higher percentages of GABAergic currents compared with other ventral interneurons. In combination, these characteristics increase inhibitory charge transfer in RCs compared with non-RCs. Given the high density of inhibitory synapses on RCs (Harrington et al., 1994), we conclude that during postnatal development, inhibitory synaptic in-

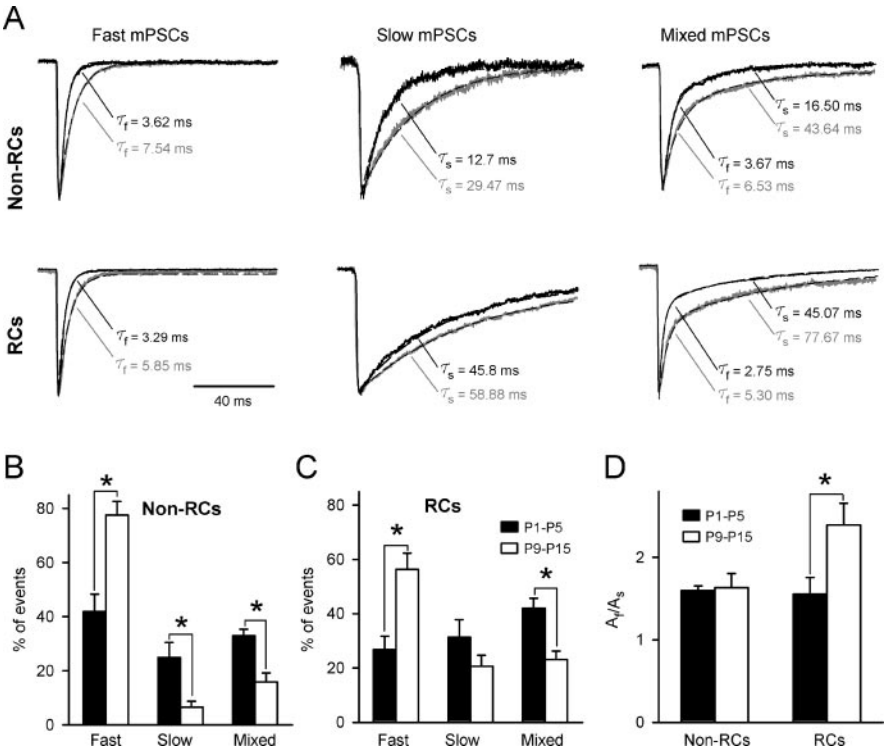

Figure 7. Postnatal development of mixed mPSCs. ***A***, Averaged fast (left), slow (middle), and mixed (right) mPSCs from one non-RC (top traces) and one RC (bottom traces) at P1–P5 (gray traces) and P9–P15 (black traces). Monoexponential or biexponential fitted curves (dashed lines) are superimposed on single events or dual-component mPSCs, respectively. Mixed mPSCs were fit by the sum of two exponential functions with time constants τ_f (for the fast component) and τ_s (for the slow component). These were similar to the decay time constants of single fast- and slow-decaying events, respectively. ***B***, ***C***, Percentages of events falling in each category in non-RCs (***B***) and RCs (***C***) from P1–P5 (■; $n = 11$ RCs and 12 non-RCs) and P9–P15 (□; $n = 10$ RCs and 10 non-RCs). The incidence of fast-decaying events increased with age in both groups, whereas slow and mixed mPSCs decreased more in non-RCs. The asterisks indicate significant differences between both age groups with $p < 0.05$ (two-way ANOVA; Duncan's test). Data are expressed as mean percentage ± SE. ***D***, Relative contributions of the fast and slow components (expressed as A_f/A_s ratio) to the peak amplitudes of mixed mPSCs. The A_f/A_s ratio was initially similar in RCs and non-RCs. With development, it remained constant in non-RCs (although the proportion of mixed events decreased), and A_f/A_s ratios increased in RCs. Data are expressed as mean ± SE. The asterisk indicates significant differences with $p < 0.05$ (two-way ANOVA; Duncan's multiple range test).

puts on RCs become greatly potentiated compared with other ventral interneurons. These functional features can be explained by the development of specific structural and molecular properties of inhibitory synapses on RCs and appear well adapted to RC function.

Maturation of postsynaptic inhibitory current peak amplitudes

The most striking feature of inhibitory synapses on RCs was the large increase in glycinergic mPSC peak amplitudes with development. The magnitude of this postnatal increase is larger than in other neurons studied previously (Gao et al., 1998, 2001; Kotak et al., 1998; Singer et al., 1998; Smith et al., 2000; Nabekura et al., 2004; Van Zundert et al., 2004) and correlates with the increase, specifically on RCs, of gephyrin clustering, a protein involved in trapping inhibitory receptors at postsynaptic densities. From P2 to P15, average gephyrin cluster size on RCs increased from 0.19 to 0.41 μm^2, and the proportion of very large clusters (>0.5 μm^2) increased from 5 to 35% (Geiman et al., 2000). These large gephyrin clusters set RCs apart from other neurons (Alvarez et al., 1997).

Larger gephyrin clusters present an opportunity for trapping and anchoring more postsynaptic receptors and increase postsynaptic currents. Indeed, average gephyrin cluster sizes were correlated with average glycinergic mPSC peak amplitudes (Lim et al., 1999; Van Zundert et al., 2004). Modification of postsynaptic receptor properties could also contribute to increased peak amplitude. However, glycine receptor properties mature similarly in RC and non-RCs. Similar studies on cranial motoneurons also concluded that receptor accumulation is the major contributor to postnatal increases in average glycinergic mPSC peak amplitude (Singer and Berger, 1999). Thus, the best explanation for the large increase in glycinergic current amplitudes in RCs is higher recruitment of glycine receptors to large postsynaptic gephyrin clusters.

Gephyrin has been also related to postsynaptic $GABA_A$ receptor clustering (Craig et al., 1996; Essrich et al., 1998; Sassoe-Pognetto and Fritschy, 2000); however, GABAergic mPSC peak amplitudes were enhanced to a smaller degree in developing RCs. GABAergic mPSC amplitudes can also increase through accumulation of postsynaptic $GABA_A$ receptors (Nusser et al., 1997, 1998), but a recent report found only weak correlation with gephyrin clustering (Levi et al., 2004). Gephyrin interactions with glycine and $GABA_A$ receptors suggest a tighter relationship between gephyrin clustering and glycine receptors than with $GABA_A$ receptors (Meyer et al., 1995; Meier et al., 2000, 2001; Dahan et al., 2003; Hanus et al., 2004). Gephyrin disruption causes complete declustering of glycine receptors (Kirsch et al., 1993; Feng et al., 1998) and loss of $GABA_A$ receptors (Essrich et al., 1998; Kneussel et al., 1999), but significant gephyrin-independent $GABA_A$ receptor clusters remain (Fischer et al., 2000; Kneussel et al., 2001; Levi et al., 2004). Moreover, during early synapse formation, postsynaptic $GABA_A$ receptors cluster postsynaptically before gephyrin (Dumoulin et al., 2000; Danglot et al., 2003; Levi et al., 2004). Thus, although gephyrin contributes to stabilize $GABA_A$ receptors at postsynaptic densities (Danglot et al., 2003), it is not always necessary for $GABA_A$ receptor postsynaptic recruitment and clustering. In addition, $GABA_A$ receptors are best stabilized by a gephyrin splice isoform containing the C5 cassette (Meier and Grantyn, 2004); therefore, postsynaptic $GABA_A$ receptor numbers and currents might be best related to the relative abundance of specific gephyrin isoforms than to overall gephyrin content.

Maturation of postsynaptic inhibitory current time course

The long time courses of $GABA_A$ postsynaptic currents are major contributors to total charge transfer underlying inhibitory currents in RCs and are well explained by the expression of $\alpha3/\alpha5$-containing $GABA_A$ receptors (Geiman et al., 2002). Recombinant $\alpha3$-containing $GABA_A$ receptors are the least sensitive to GABA (Sigel et al., 1990; Verdoorn, 1994), resulting in slower opening, deactivation, inactivation, and postsynaptic current lengthening

Table 3. Properties of mixed mPSCs

		Mixed mPSC parameters					
	n	A_f (percentage of peak)	A_s (percentage of peak)	τ_f (ms)	τ_s (ms)	Frequency (Hz)	Q (pC)
RCs							
P1–P5 ($n = 11$)	11	58 ± 4	42 ± 4	5.8 ± 0.3	65.5 ± 5.1	0.32 ± 0.08	1.72 ± 0.19
P9–P15 ($n = 12$)	12	69 ± 2*	31 ± 2*	3.5 ± 0.2*	42.6 ± 1.8*	0.24 ± 0.04	1.95 ± 0.17
Non-RCs							
P1–P5 ($n = 10$)	10	60 ± 3	40 ± 3	6.2 ± 0.3	33.2 ± 2.3§	0.30 ± 0.05	1.02 ± 0.11§
P9–P15 ($n = 10$)	10	61 ± 1§	39 ± 1§	3.9 ± 0.2*	15.8 ± 0.9*§	0.19 ± 0.04	0.64 ± 0.23§

Values are mean ± SE. The asterisks indicate significant differences ($p < 0.05$; two-way ANOVA; Duncan's multiple range test) between age groups; the § symbols indicate significant differences between RCs and non-RCs of the same age.

(Gingrich et al., 1995; Serafini et al., 1998). Decay time constant and total charge transfer in RC GABAergic mPSCs was strikingly similar to those reported in reticular thalamic (Rt) neurons (Browne et al., 2001), another neuron that expresses $\alpha3/\alpha5$ $GABA_A$ receptors. Interestingly, Rt neurons and RCs have common functional features: both provide recurrent negative feedback and respond to excitatory synaptic inputs with high-frequency burst firing. The properties of $\alpha3/\alpha5$-containing $GABA_A$ receptors might be well adapted to the common integrative properties exhibited by these cells.

Slow-decaying $GABA_A$ currents were good predictors of whether or not recorded neurons would display anatomical features of RCs. In addition, GABAergic currents decayed 25% faster in mature RCs compared with immature RCs. A parallel speeding of $GABA_A$ currents was found for the faster decays of non-RCs. These changes could suggest developmentally regulated alterations in $GABA_A$ receptor subunit structure affecting channel kinetics. Alternatively, they could be explained by alterations in receptor localization (Chery and De Koninck, 1999), β subunit phosphorylation (Hinkle and MacDonald, 2003), or GABA reuptake maturation (Draguhn and Heinemann, 1996) (but see Chery and De Koninck, 1999; Nusser and Mody, 2002; Overstreet and Westbrook, 2003). Our immunocytochemical data suggest that $GABA_A$ receptors in RCs are highly clustered at synapses in adults and neonates (Geiman et al., 2002; T. Culberston and F. J. Alvarez, unpublished observations), indicating that major developmental changes in receptor localization in RCs are unlikely. Our data also suggests that $GABA_A$ receptors in RCs contain $\beta3$ subunits (Geiman et al., 2002). Protein kinase A-dependent phosphorylation of $\beta3$ subunits slows down $GABA_A$ receptor deactivation and prolongs postsynaptic currents (Hinkle and MacDonald, 2003). In addition, neurosteroid prolongation of GABAergic currents is potent on $\beta2/3$-containing $GABA_A$ receptors (Wingrove et al., 1994). In the spinal cord, neurosteroid modulation weakens with age (Keller et al., 2004), and this decline is perhaps partly responsible for the acceleration of GABAergic currents.

A reduction in glycinergic current decay time was also observed in both RCs and non-RCs during development. A switch from neonatal $\alpha2$- to adult $\alpha1$-containing glycine receptors occurs during the first two postnatal weeks in the rat spinal cord (Akagi and Miledi, 1988; Becker et al., 1988; Malosio et al., 1991) and correlates with a decrease in glycine receptor mean open time and PSC decays (Takahashi et al., 1992; Singer et al., 1998). Decay parameters measured at P1–P5 were faster than those reported in neurons with predominant expression of $\alpha2$ glycine receptors and similar to neurons at intermediate developmental stages expressing both $\alpha1$ and $\alpha2$ glycine receptors (Singer et al., 1998; Van Zundert et al., 2004). Previously, we detected significant amounts of $\alpha1$ glycine receptors in RCs just after birth (Geiman et al., 2000). Therefore, glycinergic decay acceleration in RCs is best explained by progressive downregulation of neonatal $\alpha2$ subunits.

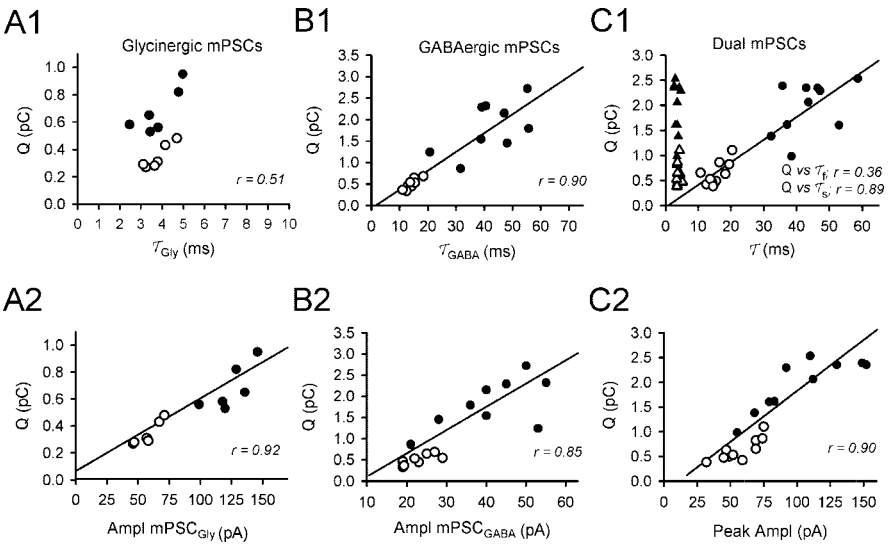

Figure 8. Charge transferred by single and mixed mPSCs. ***A1***, ***A2***, Relationships obtained between the charge transferred into the postsynaptic cell (Q; in picocoulombs) and the decay constant (***A1***; τ_{Gly}) or peak amplitude (Ampl; ***A2***) for glycinergic events in RCs (filled circles; $n = 6$) and non-RCs (open circles; $n = 6$) recorded from P9–P15 animals. Individual points correspond to average data in each neuron. ***B1***, ***B2***, Same as in ***A*** but for GABAergic mPSCs. ***C1***, ***C2***, Plots showing the relationship between the charge transfer associated with dual mPSCs and the decay constants of the fast (***C1***; filled triangles; τ_f) and slow (***C1***; open circles; τ_s) components and the peak mPSC amplitude (***C2***) in 10 RCs (filled symbols) and 10 non-RCs (open symbols) recorded at P9–P15. Correlation coefficients of the regression lines are indicated. The charge transferred was always larger in RCs than in non-RCs, each cell type forming a discrete cluster in the plots. The charge transfer in pharmacologically isolated $mPSCs_{Gly}$ correlated well with the amplitude but not the decay time. In contrast, both decay time and peak amplitudes correlated significantly with charge transfer in pharmacologically isolated $mPSCs_{GABA}$, although because of their long time courses, the correlation was better with the decay constant. In dual mPSCs, both peak amplitude (dominated by the fast glycinergic currents) and decay time (dominated by the slow GABAergic currents) correlated equally well with the total charge transferred.

Maturation of cotransmission

GABA and glycine corelease is generally demonstrated by spontaneous mPSCs displaying biphasic decays with partial time constants similar to those of GABAergic and glycinergic mPSCs. Because mPSCs are interpreted as the postsynaptic action of neurotransmitter released from single vesicles, the presence of

mixed mPSCs suggests GABA and glycine corelease from individual vesicles (Jonas et al., 1998), a possibility also supported by the use of a common vesicular transporter (Sagne et al., 1997; Chaudry et al., 1998) (but see Katsurabayashi et al., 2004). Biphasic mPSCs indicative of corelease have been shown at synapses in the spinal cord (Jonas et al., 1998; Chery and De Koninck, 1999; Gao et al., 2001; Keller et al., 2001), cerebellum (Dumuolin et al., 2001), and brainstem (O'Brien and Berger, 1999; Russier et al., 2002; Nabekura et al., 2004). A postnatal decrease in the level of cotransmission was reported for many neurons, and it is usually associated with downregulation of GABAergic currents and a switch to mainly glycine-mediated inhibitory synaptic mechanisms (Kotak et al., 1998; Gao et al., 2001; Keller et al., 2001; Nabekura et al., 2004). Most ventral interneurons show a similar developmental pattern; however, RCs were different because of the remarkable maintenance of GABAergic and mixed currents. Correspondingly, morphological data indicate that 60–75% of inhibitory terminals on adult RCs coexpress presynaptic and postsynaptic markers suggesting mixed neurotransmission, a percentage higher than in other ventral horn synapses (Geiman et al., 2002). The mechanisms that regulate the amount of cotransmission are unknown (van den Pol, 2004), but the choice has important consequences on the timing and strength of synaptic inhibition. High levels of cotransmission over RCs enhance inhibitory current strength by permitting large peak amplitudes while maintaining very slow time courses. Russier et al. (2002) showed that inhibitory synapses decreased motoneuron firing more efficiently when GABAergic and glycinergic transmission occurred simultaneously compared with experimental situations in which one or other component was blocked. Cotransmission also allowed inhibition with complementary time courses, transient by glycine and sustained by GABA.

Inhibitory modulation of RC function

The functional properties of inhibitory synaptic currents in RCs increase synaptic inhibition in amplitude and duration and develop in parallel to the spinal circuitry underlying locomotion. In the adult spinal cord, RC-mediated recurrent inhibition modulates the dynamic behavior of motoneuron firing by acting as a gain regulator of their discharge and recruitment (Windhorst, 1996; Uchiyama et al., 2003; Hultborn et al., 2004). The fine organization of recurrent inhibition on different motoneuron types and pools allows RCs to influence motoneuron firing variability, force gain, and motor discharge synchronization in homonymous and synergistic motoneuron pools and muscles. RCs also facilitate activity in antagonists through regulation of reciprocal Ia inhibitory interneurons (Hultborn et al., 1979). Thus, despite the relative simplicity of the recurrent inhibitory loop, RCs exert a variety of complex functions during motor activity. Not surprisingly recurrent inhibition is finely modulated during different motor behaviors. For example, the level of recurrent inhibition changes during voluntary movements according to the strength of muscle contraction and motor task (Hultborn and Pierrot-Deseilligny, 1979; Katz and Pierrot-Deseilligny, 1999; Iles et al., 2000). This modulation implies the existence of effective mechanisms to decouple RC firing from motor axon inputs. However, RCs receive long-lasting cholinergic EPSPs from motor axons and display unusual low thresholds for action potential generation. These peculiarities result in the characteristic tendency of RCs to discharge bursts of spikes in response to incoming motor axon volleys, even when only one action potential travels down a single motor axon (for review, see Windhorst, 1990). Modulation of RC activity therefore requires complementary well-matched inhibition. Inhibitory synapses on RCs are strategically located more proximal to the cell body than cholinergic synapses (Alvarez et al., 1999) and their synaptic structure (Alvarez et al., 1997) and molecular/neurochemical organization (Geiman et al., 2002) seem to correlate with the large amplitude and relatively long time courses of inhibitory currents described here.

In conclusion, the functional, structural, and molecular characteristics of inhibitory synapses on RCs appear well adapted to counteract robust and long-lasting motor axon-driven excitatory inputs in RCs and allow effective modulation of RC activity and recurrent inhibition of motoneurons.

References

Akagi H, Miledi R (1988) Heterogeneity of glycine receptors and their messenger RNAs in rat brain and spinal cord. Science 242:270–273.

Alvarez FJ, Dewey DE, Harrington DA, Fyffe REW (1997) Cell-type specific organization of glycine receptor clusters in the spinal mammalian spinal cord. J Comp Neurol 379:150–170.

Alvarez FJ, Dewey DE, McMillin P, Fyffe RE (1999) Distribution of cholinergic contacts on Renshaw cells in the rat spinal cord: a light microscopic study. J Physiol (Lond) 515:787–797.

Arvidsson U, Ulfhake B, Cullheim S, Ramírez V, Shupliakov O, Hökfelt T (1992) Distribution of calbindin D28k-like immunoreactivity (LI) in the monkey ventral horn: do Renshaw cells contain calbindin D28k-LI? J Neurosci 12:718–728.

Becker CM, Hoch W, Betz H (1988) Glycine receptor heterogeneity in rat spinal cord during postnatal development. EMBO J 7:3717–3726.

Browne SH, Kang J, Akk G, Chiang LW, Schulman H, Huguenard JR, Prince DA (2001) Kinetic and pharmacological properties of $GABA_A$ receptors in single thalamic neurons and $GABA_A$ subunit expression. J Neurophysiol 86:2312–2322.

Carr PA, Alvarez FJ, Leman EA, Fyffe RE (1998) Calbindin D28k expression in immunohistochemically identified Renshaw cells. NeuroReport 9:2657–2661.

Chaudhry FA, Reimer RJ, Bellocchio EE, Danbolt NC, Osen KK, Edwards RH, Storm-Matisen J (1998) The vesicular GABA transporter, VGAT, localizes to synaptic vesicles in sets of glycinergic as well as GABAergic neurons. J Neurosci 18:9733–9750.

Chery N, De Koninck Y (1999) Junctional versus extrajunctional glycine and $GABA_A$ receptor-mediated IPSCs in identified lamina I neurons of the adult rat spinal cord. J Neurosci 19:7342–7355.

Craig AM, Banker G, Chang W, McGrath ME, Serpinskaya AS (1996) Clustering of gephyrin at GABAergic but not glutamatergic synapses in cultured rat hippocampal neurons. J Neurosci 16:3166–3177.

Dahan M, Levi S, Luccardini C, Rostaing P, Riveau B, Triller A (2003) Diffusion dynamics of glycine receptors revealed by single-quantum dot tracking. Science 302:442–445.

Danglot L, Triller A, Bessis A (2003) Association of gephyrin with synaptic and extrasynaptic $GABA_A$ receptors varies during development in cultured hippocampal neurons. Mol Cell Neurosci 23:264–278.

Dourado M, Sargent PB (2002) Properties of nicotinic receptors underlying Renshaw cell excitation by alpha-motor neurons in the neonatal spinal cord. J Neurophysiol 87:3117–3125.

Draguhn A, Heinemann U (1996) Different mechanisms regulate IPSC kinetics in early postnatal and juvenile hippocampal granule cells. J Neurophysiol 76:3983–3993.

Dumoulin A, Levi S, Riveau B, Gasnier B, Triller A (2000) Formation of mixed glycine and GABAergic synapses in cultured spinal cord neurons. Eur J Neurosci 12:3883–3892.

Dumoulin A, Triller A, Dieudonne S (2001) IPSC kinetics at identified GABAergic and mixed GABAergic and glycinergic synapses onto cerebellar Golgi cells. J Neurosci 21:6045–6057.

Eccles JC, Fatt P, Koketsu K (1954) Cholinergic and inhibitory synapses in a pathway from motor-axon collaterals to motoneurones. J Physiol (Lond) 126:524–562.

Essrich C, Lorez M, Benson JA, Fritschy JM, Luscher B (1998) Postsynaptic clustering of major $GABA_A$ receptor subtypes requires the gamma 2 subunit and gephyrin. Nat Neurosci 1:563–571.

Feng G, Tintrup H, Kirsch J, Nichol MC, Kuhse J, Betz H, Sanes JR (1998) Dual requirement for gephyrin in glycine receptor clustering and molybdoenzyme activity. Science 282:1321–1324.

Fischer F, Kneussel M, Tintrup H, Haverkamp S, Rauen T, Betz H, Wassle H (2000) Reduced synaptic clustering of GABA and glycine receptors in the retina of the gephyrin null mutant mouse. J Comp Neurol 427:634–648.

Fyffe RE (1990) Evidence for separate morphological classes of Renshaw cells in the cat's spinal cord. Brain Res 536:301–304.

Gao BX, Cheng G, Ziskind-Conhaim L (1998) Development of spontaneous synaptic transmission in the rat spinal cord. J Neurophysiol 79:2277–2287.

Gao BX, Stricker C, Ziskind-Conhaim L (2001) Transition from GABAergic to glycinergic synaptic transmission in newly formed spinal networks. J Neurophysiol 86:492–502.

Geiman EJ, Knox MC, Alvarez FJ (2000) Postnatal maturation of gephyrin/glycine receptor clusters on developing Renshaw cells. J Comp Neurol 426:130–142.

Geiman EJ, Zheng W, Fritschy JM, Alvarez FJ (2002) Glycine and $GABA_A$ receptor subunits on Renshaw cells: relationship with presynaptic neurotransmitters and postsynaptic gephyrin clusters. J Comp Neurol 444:275–289.

Gingrich KJ, Roberts WA, Kass RS (1995) Dependence of the $GABA_A$ receptor gating kinetics on the alpha-subunit isoform: implications for structure-function relations and synaptic transmission. J Physiol (Lond) 489:529–543.

Hanus C, Vannier C, Triller A (2004) Intracellular association of glycine receptor with gephyrin increases its plasma membrane accumulation rate. J Neurosci 24:1119–1128.

Harrington DA, Alvarez FJ, Fyffe REW (1994) Somatic membrane covering by glycinergic terminals and glycine receptors of α-motoneurons and Renshaw cells in cat spinal cord. Soc Neurosci Abstr 20:1588.

Hinkle DJ, MacDonald RL (2003) β Subunit phosphorylation selectively increases fast desensitization and prolongs deactivation of $\alpha1\beta1\gamma2$L and $\alpha1\beta3\gamma2$L $GABA_A$ receptor currents. J Neurosci 23:11698–16710.

Hultborn H, Pierrot-Deseilligny E (1979) Changes in recurrent inhibition during voluntary soleus contractions in man studied by an H-reflex technique. J Physiol (Lond) 297:229–251.

Hultborn H, Lindstrom S, Wigstrom H (1979) On the function of recurrent inhibition in the spinal cord. Exp Brain Res 37:399–403.

Hultborn H, Brownstone RB, Toth TI, Gossard JP (2004) Key mechanisms for setting the input-output gain across the motoneuron pool. Prog Brain Res 143:777–795.

Iles JF, Ali A, Pardoe J (2000) Task-related changes of transmission in the pathway of heteronymous spinal recurrent inhibition from soleus to quadriceps motor neurones in man. Brain 123:2264–2272.

Jankowska E, Lindstrom S (1971) Morphological identification of Renshaw cells. Acta Physiol Scand 81:428–430.

Jonas P, Bischofberger J, Sandkuhler J (1998) Corelease of two fast neurotransmitters at a central synapse. Science 281:419–424.

Katsurabayashi S, Kubota H, Higashi H, Akaike N, Ito Y (2004) Distinct profiles of refilling of inhibitory neurotransmitters into presynaptic terminals projecting to spinal neurones in immature rats. J Physiol (Lond) 560:469–478.

Katz R, Pierrot-Deseilligny E (1999) Recurrent inhibition in humans. Prog Neurobiol 57:325–355.

Keller AF, Coull JA, Chery N, Poisbeau P, De Koninck Y (2001) Region-specific developmental specialization of GABA–glycine cosynapses in laminas I–II of the rat spinal dorsal horn. J Neurosci 21:7871–7880.

Keller AF, Breton JD, Schlichter R, Poisbeau P (2004) Production of 5α-reduced neurosteroids is developmentally regulated and shapes $GABA_A$ miniature IPSCs in lamina II of the spinal cord. J Neurosci 24:907–915.

Kirsch J, Betz H (1993) Widespread expression of gephyrin, a putative glycine receptor-tubulin linker protein, in rat brain. Brain Res 621:301–310.

Kirsch J, Wolters I, Triller A, Betz H (1993) Gephyrin antisense oligonucleotides prevent glycine receptor clustering in spinal neurons. Nature 366:745–748.

Kneussel M, Brandstatter JH, Laube B, Stahl S, Muller U, Betz H (1999) Loss of postsynaptic $GABA_A$ receptor clustering in gephyrin-deficient mice. J Neurosci 19:9289–9297.

Kneussel M, Brandstatter JH, Gasnier B, Feng G, Sanes JR, Betz H (2001) Gephyrin-independent clustering of postsynaptic $GABA_A$ receptor subtypes. Mol Cell Neurosci 17:973–982.

Kotak VC, Korada S, Schwartz IR, Sanes DH (1998) A developmental shift from GABAergic to glycinergic transmission in the central auditory system. J Neurosci 18:4646–4655.

Levi S, Logan SM, Tovar KR, Craig AM (2004) Gephyrin is critical for glycine receptor clustering but not for the formation of functional GABAergic synapses in hippocampal neurons. J Neurosci 24:207–217.

Lim R, Alvarez FJ, Walmsley B (1999) Quantal size is correlated with receptor cluster area at glycinergic synapses in the rat brainstem. J Physiol (Lond) 516:505–512.

Malosio ML, Marqueze-Pouey B, Kuhse J, Betz H (1991) Widespread expression of glycine receptor subunit mRNAs in the adult and developing rat brain. EMBO J 10:2401–2409.

Meier J, Grantyn R (2004) A gephyrin-related mechanism restraining glycine receptor anchoring at GABAergic synapses. J Neurosci 24:1398–1405.

Meier J, Meunier-Durmort C, Forest C, Triller A, Vannier C (2000) Formation of glycine receptor clusters and their accumulation at synapses. J Cell Sci 113:2783–2795.

Meier J, Vannier C, Serge A, Triller A, Choquet D (2001) Fast and reversible trapping of surface glycine receptors by gephyrin. Nat Neurosci 4:253–260.

Meyer G, Kirsch J, Betz H, Langosch D (1995) Identification of a gephyrin binding motif on the glycine receptor beta subunit. Neuron 15:563–572.

Nabekura J, Katsurabayashi S, Kakazu Y, Shibata S, Matsubara A, Jinno S, Mizoguchi Y, Sasaki A, Ishibashi H (2004) Developmental switch from GABA to glycine release in single central synaptic terminals. Nat Neurosci 7:17–23.

Nusser Z, Mody I (2002) Selective modulation of tonic and phasic inhibitions in dentate gyrus granule cells. J Neurophysiol 87:2624–2628.

Nusser Z, Cull-Candy S, Farrant M (1997) Differences in synaptic $GABA_A$ receptor number underlie variation in GABA mini amplitude. Neuron 19:697–709.

Nusser Z, Hajos N, Somogyi P, Mody I (1998) Increased number of synaptic $GABA_A$ receptors underlies potentiation at hippocampal inhibitory synapses. Nature 395:172–177.

O'Brien JA, Berger AJ (1999) Cotransmission of GABA and glycine to brain stem motoneurons. J Neurophysiol 82:1638–1641.

Oleskevich S, Alvarez FJ, Walmsley B (1999) Glycinergic miniature synaptic currents and receptor cluster sizes differ between spinal cord interneurons. J Neurophysiol 82:312–319.

Overstreet LS, Westbrook GL (2003) Synapse density regulates independence at unitary inhibitory synapses. J Neurosci 23:2618–2626.

Pouille F, Scanziani M (2001) Enforcement of temporal fidelity in pyramidal cells by somatic feed-forward inhibition. Science 293:1159–1163.

Renshaw B (1946) Central effects of centripetal impulses in axons of spinal central roots. J Neurophysiol 9:191–204.

Russier M, Kopysova IL, Ankri N, Ferrand N, Debanne D (2002) GABA and glycine co-release optimizes functional inhibition in rat brainstem motoneurons in vitro. J Physiol (Lond) 541:123–137.

Sagne C, El Mestikawy S, Isambert MF, Hamon M, Henry JP, Giros B, Gasnier B (1997) Cloning of a functional vesicular GABA and glycine transporter by screening of genome databases. FEBS Lett 417:177–183.

Sassoe-Pognetto M, Fritschy JM (2000) Mini-review: gephyrin, a major postsynaptic protein of GABAergic synapses. Eur J Neurosci 12:2205–2210.

Semyanov A, Walker MC, Kullmann DM, Silver RA (2004) Tonically active $GABA_A$ receptors: modulating gain and maintaining the tone. Trends Neurosci 27:262–269.

Serafini R, Maric D, Maric I, Ma W, Fritschy JM, Zhang L, Barker JL (1998) Dominant $GABA_A$ receptor/Cl^- channel kinetics correlate with the relative expressions of alpha2, alpha3, alpha5 and beta3 subunits in embryonic rat neurones. Eur J Neurosci 10:334–349.

Sigel E, Baur R, Trube G, Mohler H, Malherbe P (1990) The effect of subunit composition of rat brain $GABA_A$ receptors on channel function. Neuron 5:703–711.

Singer JH, Berger AJ (1999) Contribution of single-channel properties to the time course and amplitude variance of quantal glycine currents recorded in rat motoneurons. J Neurophysiol 81:1608–1616.

Singer JH, Talley EM, Bayliss DA, Berger AJ (1998) Development of glycinergic synaptic transmission to rat brain stem motoneurons. J Neurophysiol 80:2608–2620.

Smith AJ, Owens S, Forsythe ID (2000) Characterisation of inhibitory and excitatory postsynaptic currents of the rat medial superior olive. J Physiol (Lond) 529:681–698.

Takahashi T, Momiyama A, Hirai K, Hishinuma F, Akagi H (1992) Functional correlation of fetal and adult forms of glycine receptors with devel-

opmental changes in inhibitory synaptic receptor channels. Neuron 9:1155–1161.

Thomas RC, Wilson VJ (1965) Precise location of Renshaw cells with a new marking technique. Nature 206:211–213.

Turrigiano GG, Nelson SB (2004) Homeostatic plasticity in the developing nervous system. Nat Rev Neurosci 5:97–107.

Uchiyama T, Johansson H, Windhorst U (2003) A model of the feline medial gastrocnemius motoneuron-muscle system subjected to recurrent inhibition. Biol Cybern 89:139–151.

van den Pol AN (2004) Developing neurons make the switch. Nat Neurosci 7:7–8.

Van Zundert B, Alvarez FJ, Tapia JC, Yeh HH, Diaz E, Aguayo LG (2004) Developmental-dependent action of microtubule depolymerization on the function and structure of synaptic glycine receptor clusters in spinal neurons. J Neurophysiol 91:1036–1049.

Verdoorn TA (1994) Formation of heteromeric gamma-aminobutyric acid type A receptors containing two different alpha subunits. Mol Pharmacol 45:475–480.

Vicini S, Ferguson C, Prybylowski K, Kralic J, Morrow AL, Homanics GE (2001) $GABA_A$ receptor $\alpha 1$ subunit deletion prevents developmental changes of inhibitory synaptic currents in cerebellar neurons. J Neurosci 21:3009–3016.

Windhorst U (1990) Activation of Renshaw cells. Prog Neurobiol 35:135–179.

Windhorst U (1996) On the role of recurrent inhibitory feedback in motor control. Prog Neurobiol 49:517–587.

Wingrove PB, Wafford KA, Bain C, Whiting PJ (1994) The modulatory action of loreclezole at the gamma-aminobutyric acid type A receptor is determined by a single amino acid in the beta 2 and beta 3 subunit. Proc Natl Acad Sci USA 91:4569–4573.